UNIVERSITA' POLITECNICA DELLE MARCHE

FACOLTA' DI INGEGNERIA

Corso di Laurea magistrale in Biomedical Engineering

Analysis of resting-state fMRI images to study the interhemispherical functional connectivity

Relatore:

Prof. Mara Fabri

Tesi di Laurea di:

Giusi Piccolantonio

Correlatore:

Prof. Gabriele Polonara

A.A. 2020/2021

Alla mia famiglia

Contents

Abbreviations

AC Anterior Commissure

AgCC Agenesis of Corpus Callosum

BA Brodmann Area

BET Brain Extraction Tool

BOLD Blood-Oxygen-Level Dependent

BSS Blind Source Separation

BV BrainVoyager

CBF Cerebral Blood Flow

CBV Cerebral Blood Volume

CC Corpus Callosum

CSF CerebroSpinal Fluid

dHb Deoxyhemoglobin

DMN Default Mode Network

FC Functional Connectivity

fMRI Functional Magnetic Resonance Imaging

FSL FMRIB Software Library

GM Grey Matter

Hb Hemoglobin

HbO_2 Oxyhemoglobin

HR Hemodynamic Response

IC Independent Component

ICA Independent Component Analysis

MNI Montreal Neurological Institute

MRI Magnetic Resonance Imaging

N-IC Noise Independent Component

PC Posterior Commissure

PET Positron Emission Tomography

rs-fMRI Resting-State Functional Magnetic Resonance Imaging

RSNs Resting State Networks

SI Primary Somatosensory cortex

SII Secondary Somatosensory cortex

S-IC Signal Independent Component

SMA Supplementary Motor Area

TE Echo Time

TR Repetition Time

WM White Matter

1. Introduction

The corpus callosum (CC) is the largest white matter structure in the human brain, about ten centimetres in length and consisting of 200-300 million of axonal projections. This thick bundle of commissural fibres is located deep in the brain, beneath the cerebral cortex. The CC connects the two halves of the brain, the right and left hemispheres, and allows both hemispheres to communicate and send neural signals to each other. In this way, sensory, motor, and cognitive information's are continuously exchanged between the two hemispheres via this neural pathway. Consequently, a damage to the CC can lead to incorrect hemispheres communication and loss of functions as the visual perception, speech, and memory.

In the past, it was necessary to intervene by cutting the CC to treat severe epilepsy. Epilepsy is a chronic condition that causes intense and recurrent seizures in the patient's brain, generally treated with medications. When the patient did not respond to anti-seizure medications, callosotomy was used.

1.1 Callosotomy

In the 1940s, the first case of corpus callosotomy was performed by Dr. William P. Van Wagenen. The callosotomy, often called split-brain surgery, is a palliative surgical procedure used as a treatment of intractable epilepsy. The corpus callosum is cut to interrupt the interhemispheric spread of epileptic seizures (Van Wagenen and Herren, 1940). Therefore, this invasive treatment allows patients to return to a normal life after the operation. Nowadays the split-brain surgery is completely replaced by more effective anticonvulsant drugs, and, if necessary, by selective and less radical surgery (Pearce, 2019).

In the last years of 1950, Roger Sperry began his research on split-brain to study the functional differences between the left and right brain hemispheres. At that point of time, based on previous studies about lateralization of brain functions (for example, the language and speech areas are usually located in the left hemisphere (Broca, 1865), Sperry was knowing that certain brain functions are localized largely in one hemisphere versus the other: each hemisphere controls movement and vision of the opposite side of the body, so that the left hemisphere is responsible for the right eye and controls the movement of the right part of the body and vice versa (Lienhard, 2017).

Initially, Sperry performed experiments by cutting the CC of cats first and then of monkeys. As a result of these experiments, he deduced that these split-brain mammals were able to learn and memorize two different events, but each hemisphere was unable to communicate the acquired information; this led Sperry to assume that the two hemispheres function separately when are not connected by the CC, which therefore makes them act as a single brain (Sperry, 1961).

In the 1960s, Sperry carried out the first studies on human patients. After callosotomy, the split-brain patients did not show any significant difference in function and behaviour from people with intact CC. So, he wondered: if the surgery did not affect the patient's normal activity, then what is the role of the CC? Thus, Sperry and his graduate student Michael Gazzaniga invited several split-brain patients to participate in their study. They designed a series of tests to investigate if and what changes occurred in callosotomized patients, by testing their language, vision, and motor skills (Gazzaniga et al., 1965; Sperry, 1968).

To evaluate the functional capacity of each hemisphere, it is critical to provide information to one side of the brain only.

In the first test, the split-brain patients had to look at a white screen with a black cross or dot in the middle, which acts as a dividing point for the patient's visual field; in this way, the left hemisphere processed what was shown in the right visual field (so the right of the cross) and vice versa. On the screen, Sperry presented a word to the left or right visual field for a second and then asked the patients to tell him the word they had read on the screen, as showed in Figure 1.1. It turned out that when the word was presented in the right visual field, and

thus processed by the left hemisphere, the patients were able to repeat the displayed word. Conversely, when the word was shown in the left visual field, and thus processed by the right hemisphere, the patients were unable to report the word. This led Sperry to assume that the language center is only in the left hemisphere.

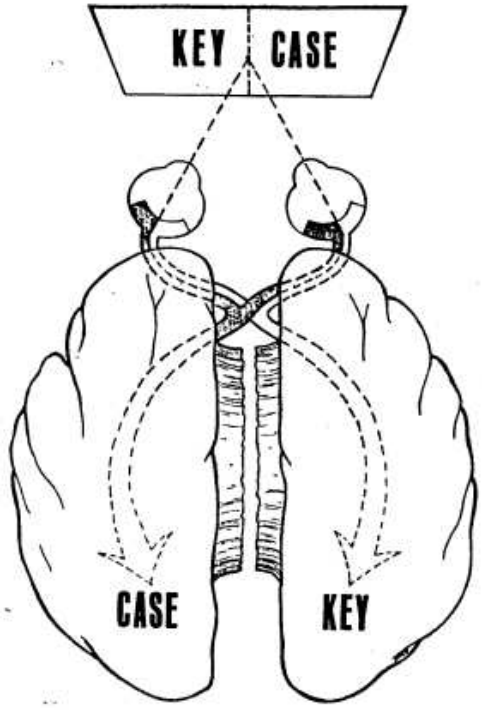

Figure 1.1. Two words were displayed in right and left side of a central dot. The word displayed in the left visual field was processed by the right hemisphere and vice versa (Sperry, 1968).

In the follow-up experiment, Sperry and Gazzaniga were focused on the function of the right hemisphere, to investigate if the split-brain patients had some language and memory abilities or at least recognize the word on the left side of the white screen. In this second test, after presenting two different words, on in the left and the other in the right visual field, Sperry asked the patients which word they had read and, as expected, they only reported the word displayed on the right side of the screen. Then, Sperry asked them to close their eyes and draw with their left hand, controlled by the right hemisphere. The patients drew the word displayed on the left side of the screen, so processed in the right hemisphere; when they looked at the drawing, they had no idea why the drawing did not correspond to the read word.

Sperry carried out another experiment, similar to the second test, to continue studying the right hemisphere's ability to recognize words. Sperry asked the patients to place their left hand in a tray full of different objects (not visible to the patients). A word or an image, which indicated one object on the tray, was shown on the left visual field and so processed by the right hemisphere. The patients were asked to take an object from the tray by using the left hand, as showed in Figure 1.2. The patients picked up the object corresponding to the showed word/image, but they couldn't name the object and didn't even know why they chose that object. Sperry noticed that the patients, despite ignoring the object's name, were able to give a very rudimentary description of the object itself, for example "the object is round" instead of "the object is a ball". That was a great achievement, as until that time it was supposed that the language skills were only placed in the left hemisphere; however, from this last study, it was found that also the right hemisphere had some language ability, although elementary and rough.

Sperry concluded that the left hemisphere contains the language center, and it is also responsible for understanding and remembering the words; the right hemisphere could recognize the words and was the source of emotional colouring of language. Actually, the left hand drew and picked up the object designed by the word showed in the left visual field and processed in the right hemisphere; the patient and also gave a basic description of it but was unable to pronounce the word. Moreover, these tests demonstrated that when the CC is severed, the two hemispheres are incapable to share the information; however, each hemisphere is still able to memorize and learn, but it has no idea what the other is doing (Gazzaniga et al., 1965; Sperry, 1968).

Sperry and his colleagues received the Nobel Prize in Physiology and Medicine in 1981 for their split-brain research and for the findings regarding the lateralization of the cerebral hemispheres.

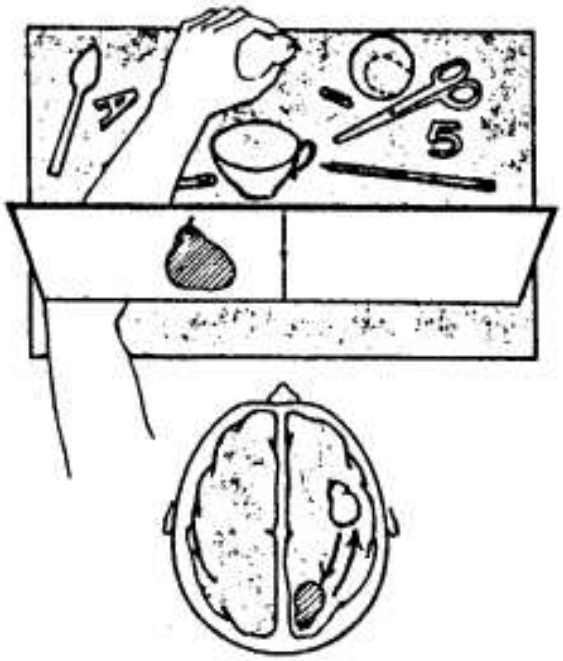

Figure 1.2. A word/image was displayed on the left side of the screen. By using the left hand, the subject picked up the object described on the screen and processed by the right hemisphere (Sperry, 1968).

1.2 Functional Magnetic Resonance Imaging

In the first years of 1990, Seiji Ogawa and Kenneth Kwong discovered a new non-invasive technique to study brain activity by measuring changes in blood flow: functional Magnetic Resonance Imaging (fMRI; Ogawa et al., 1990a). Functional MRI is used in clinical settings, as in neurosurgery for pre-surgical planning and intraoperative monitoring of the brain areas (awake surgery), and it allows the programming of the surgical strategy to minimize the risks of post-operative deficit. However, fMRI is mainly used as a fundamental research tool, widely used in the neurological and cognitive neuroscience fields to study the different cognitive processes (language, attention, memory) in normal and pathological subjects. The main purpose of the fMRI studies is to identify the areas of the brain activated during predefined stimulation tasks, in an easily interpretable and reproducible way. This technique presents precious features compared to other methods as PET, EEG, and MEG. First, has a high spatial

resolution down to mm, is non-invasive and harmless (does not use the ionizing radiation as PET). Its limitation is a low temporal resolution (seconds; Poldrack et al., 2011).

1.2.1 fMRI basic principles

The brain needs nutrients such as oxygen and glucose to function. It consumes a large amount of the body's energy but does not have a reservoir of stored energy. During the execution of a certain task, be it motor, cognitive or sensory, neurons implicated in that task send more signals than during the rest condition. The brain areas involved in the task are more active, and here an augment of blood flow is occurring. This means that an increase in neural activity leads to greater demand for energy. The oxygen is transported in the blood bound to hemoglobin (Hb) and is characterized by low solubility. The hemodynamic response (HR) allows a rapid delivery of blood, and therefore oxygen, to the active neuronal tissues. Therefore, changes in brain activity are closely related to changes in blood flow in the same area. The modification of the oxygenation state of hemoglobin in red blood cells is the core principle of the BOLD effect, i.e., *Blood Oxygenation Level Dependent*. The most common approach towards fMRI uses the BOLD contrast, which measures the ratio of oxygenated and deoxygenated hemoglobin concentration in the blood (Ogawa et al., 1990a). Thus, by measuring the change in blood oxygenation in response to neural firing, it is possible, through the BOLD fMRI, to identify brain areas activated by certain stimuli.
As discovered by Pauling in 1936 (Pauling and Coryell, 1936), hemoglobin exists in two different stages, each with different magnetic properties:

- Oxygenated hemoglobin, known as *oxyhemoglobin* (HbO_2), presents diamagnetic characteristics, that is, it does not have unpaired electrons and the magnetic moments equals zero. HbO_2 in a blood vessel has equal susceptibility as other brain tissues, demonstrating minimal impact on the magnetic field of an MRI scanner, leading to no distortions in the MR signal.

- Deoxygenated hemoglobin, known as *deoxyhemoglobin* (dHb), presents paramagnetic characteristics, that is, it has unpaired electrons and a non-zero magnetic moment. dHb alters the susceptibility of the blood, with a magnetic susceptibility X_m, and interacts with the magnetic field of an MRI scanner resulting in local magnetic field distortions. This means that dHb suppresses the MR signal.

Based on the study of Pauling, Ogawa had the idea of combining the MRI technique (used to study the anatomy of the brain) and the magnetic properties of hemoglobin (Osawa et al., 1990b) to map functional brain activity using dHb as contrast agent, which is a natural and not a radioactive agent, at variance with PET. Note that this technique does not measure neural activity directly, but it exploits the hemodynamic variations produced by neural activity to identify the activated areas of the brain.

When neurons start to fire and neural activity in a cortical region increases, a systematic series of physiological changes occurs: first, an increase in the oxygen demands, leading to a vasodilatation and to an augment in the local cerebral blood flow (CBF), and local cerebral blood volume (CBV). As CBF increases more than the CBV, the change in blood flow exceeds the metabolic demand and, at the capillary level, there is a net increase in HbO_2 concentration whereas the dHb concentration decreases. The decrease of dHb in a cortical region has a direct effect on the signal used to produce MR images, as showed in Figure 1.3. The MR signal from that region decays less rapidly, leading to a more uniform magnetic field and therefore a stronger BOLD signal, with the result that the activated region will appear as more intense region on the functional MR images (Gore, 2003).

Therefore, the BOLD contrast relies on two principles:

I. hemoglobin can distort the magnetic field of MRI scanner in a region of the cortex according to its level of oxygenation.
II. regional blood oxygenation varies according to the levels of neural activity.

Functional MRI, thanks to the ability to acquire images in very reduced time (in the order of hundredths of a second), allows to visualise in an accurate and detailed manner the hemodynamic variations from the cortical regions, in relation to the level of neural activity in the same regions.

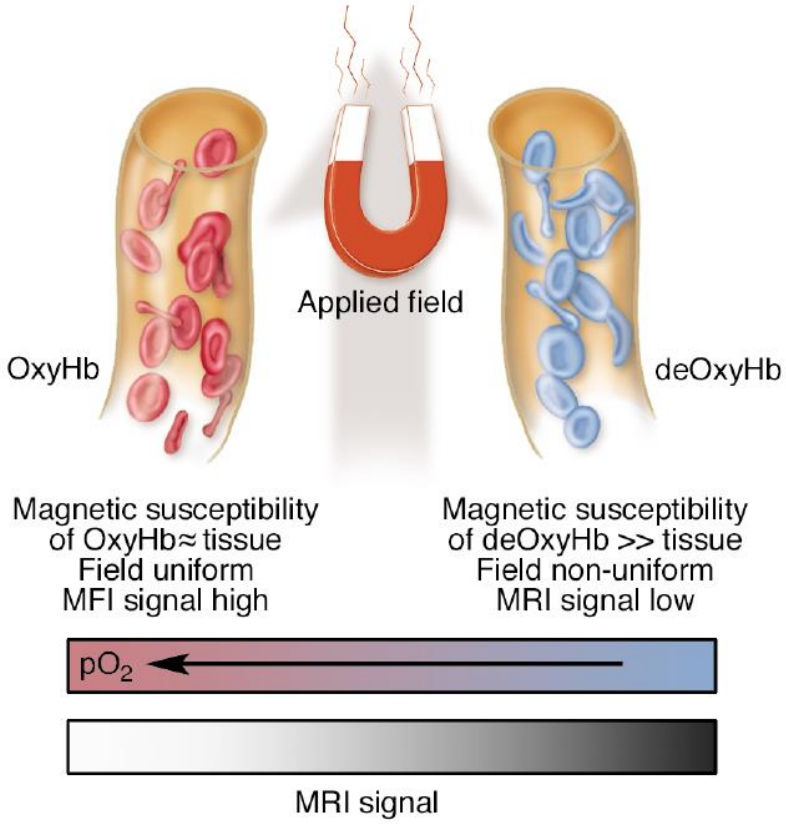

Figure 1.3. Schematic illustration of the origin of the BOLD effect in fMRI (Gore, 2003).

Thus, exploiting the hemodynamic response produced by the neuronal activity, fMRI can identify which areas of the brain are activated as a result of a particular stimulation. The trend of the BOLD signal (Figure 1.4) is strictly related to the metabolic phenomena involved in neuronal activation (Siero et al., 2013).

A typical BOLD response to a stimulus is characterized by three phases:

- Initial dip: 1-2 seconds after the neural activity, the signal drop below the baseline because an initial increase in dHb concentration occurs because of the extraction of oxygen from capillaries.

- Peak: the signal increase, reaching the peak around the 5-6 seconds following the stimulus (the vasodilation necessary to augment flow towards that cortical region requires a few seconds), caused by the increase in CBV, CBF and Hb concentration which exceeds the demands leading to a decrease in dHb concentration in the involved area. This corresponds to an increase in the BOLD ratio.

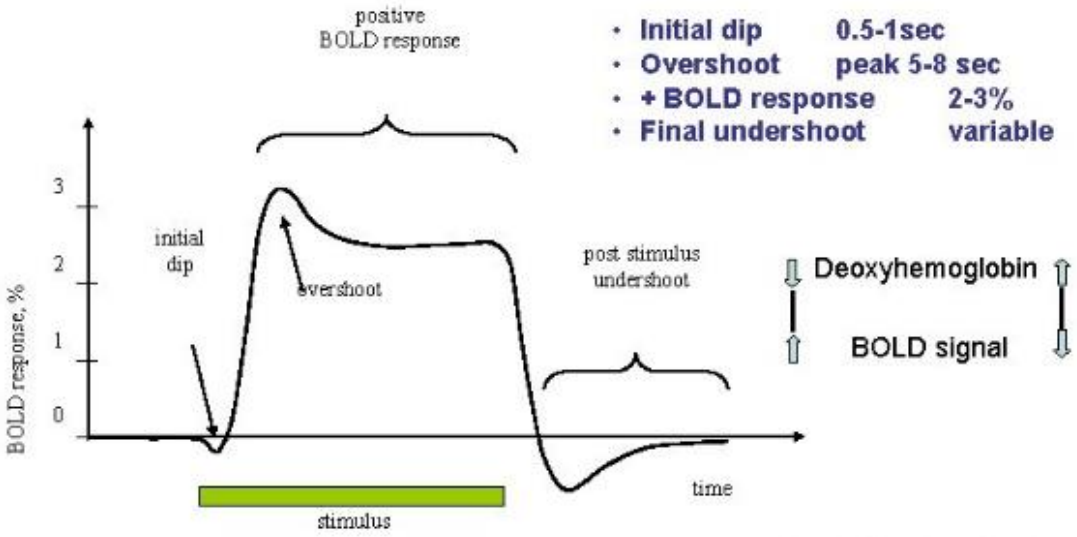

Figure 1.4. A typical MRI BOLD response model (Jezzard et al., 2001).

- Plateau: if the neural activity remains over time, then the peak value is maintained.
- Undershoot: after the peak and plateau phases, the metabolism of active neurons causes a continuous consumption of oxygen which in turn leads to an increase in dHb concentration which causes a reduction of the signal until a minimum, below the baseline. After reaching the minimum, the signal starts to increase again until it stabilizes on the basal level, prior to activation.

1.3 Resting state fMRI

It is known that hemodynamic variations in brain structures are closely related to neural activity. Recent studies performed with fMRI and PET have shown that most of brain energy consumption is spent for an intrinsic metabolic activity not related to sensory, visual or motor stimuli. These findings suggested that the brain is mainly triggered by its intrinsic activity, which external stimuli can modulate rather than determine. Therefore, the neuroscientists were interested in understanding the nature of this intrinsic activity present even at rest (when the subject is lying and relaxed).

The brain represents only 2% of the total mass of the body and consumes 20% of body's energy, most of which is used to fuel the continuous activity of neurons. In fact, the brain is always active, even in the absence of specific tasks. The increases in neuronal metabolism in the presence of functional tasks are usually much lower (<5%) than the energy consumption at rest. It has been hypothesized that this energy consumption reflects activity during rest, which decreases only when metabolic resources are temporarily redistributed for the execution of cognitive tasks (Fox and Raichle, 2007).

The fMRI offers the possibility to record the simultaneous activation of multiple brain regions highlighting neural networks, usually called functional networks or just networks. These networks are sets of regions that coactivate and/or interact in the execution of specific functions. The coactivation is measured as a synchronization of the activity in a brain region during the performance of a function, i.e., in a correlation of their activity over time. By the use of fMRI, the temporal correlation of neural activity between spatially distinct brain regions can be evaluated; this correlation is defined Functional Connectivity (FC). Regions that simultaneously modulate their activation are therefore said to be functionally connected (Fox and Raichle, 2007). Note that not all regions anatomically connected to an active region are necessarily activated as well and, at the same time, brain regions that do not have direct anatomical connections can be coactivated since they can receive signals from intermediate regions.

In the 90's, Biswal and his colleagues used fMRI technique to investigate how different areas of the brain were able to communicate with each other (Biswal et al., 1995). It was observed that, since brain activity is present even in the absence of a task or external stimuli, the fMRI signal of each region is characterized by *spontaneous fluctuations*. The brain activity not related to tasks is not a random noise, but it reflects a functional organization of the brain, suggesting that the networks are organized in a coherent way; this has generated a new avenue in neuroimaging research (Fox and Raichle, 2007).

This approach is known as resting-state fMRI (rs-fMRI), which, at variance with the task fMRI, analyses spontaneous fluctuations using BOLD contrast without requiring subjects to perform a task. The need to understand neural organization has brought interest to study resting-state patterns of the brain. Nowadays, in fact, there is a growth in the application of rs-fMRI to examine functional connectivity, both in normal and pathological conditions. Moreover, resting state studies present some advantages in comparison with task fMRI events. Actually, the absence of a specific task allows the scan of a variety of populations, such as children or cognitive impaired patients, which are not able to adhere to a specific paradigm. The time duration is about 5-10 minutes and different networks can be extracted from a single scan. In the most typical resting-state fMRI design, subjects keep their eyes closed, are instructed to not fall asleep and to think about anything. In addition, there are studies where participants keep their eyes open by fixating an object during the scanning (Barkhof et al., 2014).

The spontaneous activity during the execution of a task shows an anatomical distribution similar to that observed during the rest phase. Smith and his colleagues (Smith et al., 2009) suggested that the measured neuronal responses represent an approximately linear overlap of task-related neuronal activity and spontaneous activity. The correlation between two or more regions equally activated by the execution of a task increases during the conditions of activity, and the correlation between the other regions decreases. Therefore, the correlation between brain structures remains constant during the rest and task phase and the observed changes in the correlations are simple due to a

superimposition of spontaneous and task-related activity (Fox and Raichle, 2007).

1.3.1 Resting state networks

Resting state fMRI studies allowed researchers to identify several networks across different subjects which are denominated "resting-state networks" (RSNs). The most common RSNs identified are discovered by Beckmann and coworkers (Beckmann et al., 2005) and Smith and coworkers (Smith et al., 2009).

Beckmann and coworkers (2005) studying ten healthy subjects during rest condition, identified eight maps corresponding to eight RSNs. Figure 1.5 shows sagittal, coronal, and axial slices for eight networks overlayed onto the mean subjects' high-resolution structural image (1×1×1.5 mm), aligned to the MNI template. All coordinates are in mm from the anterior commissure.

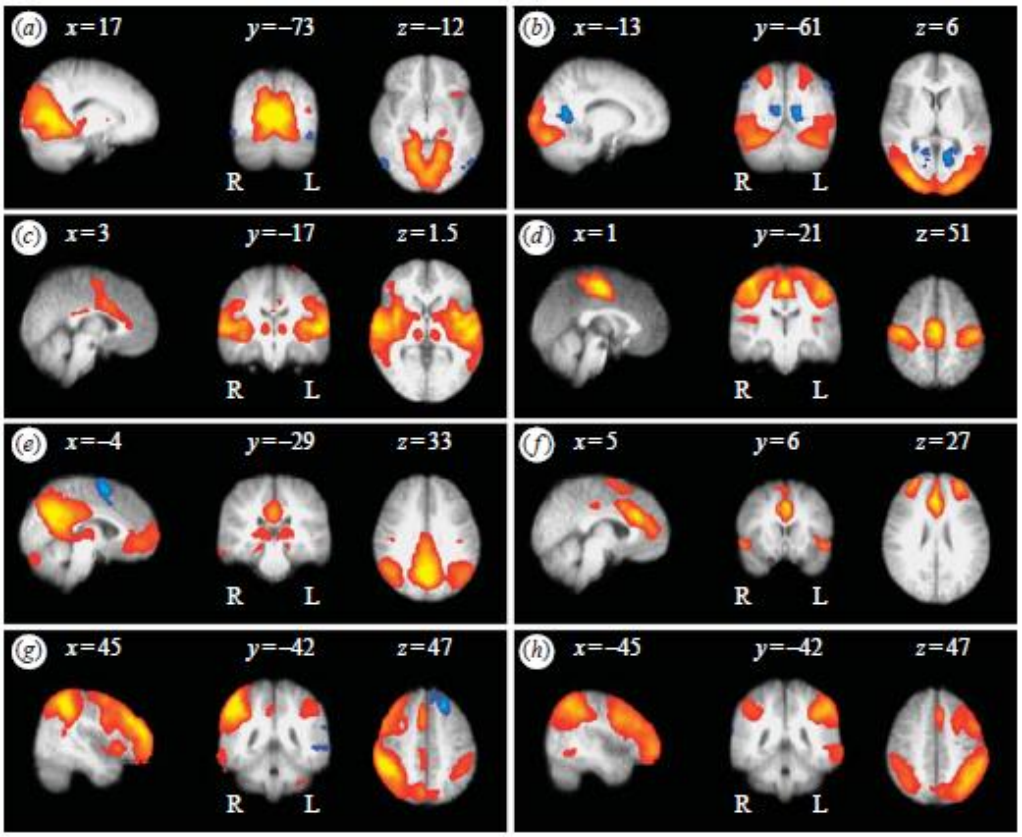

Figure 1.5. Sagittal, coronal, and axial views of different spatial maps associated with low frequency resting patterns estimated from a group of 10 subjects (Beckmann et al., 2005).

The identified maps are:

a) Medial visual cortical areas
b) Lateral visual cortical areas
c) Auditory system
d) Sensory-motor system
e) Visuo-spatial system
f) Executive control
g) Dorsal visual stream right
h) Dorsal visual stream left.

In 2009, Smith and coworkers compared the networks obtained from 36 healthy subjects during resting fMRI and those obtained from the large database of BrainMap, acquired during task fMRI. They performed a comparison between networks activated at rest and networks activated during a task to test whether there were or not a correlation between networks activated at rest and under stimuli. They identified 10 maps (Figure 1.6) corresponding to the 8 RSN maps previously described, an additional cerebellar map, and 2 distinct maps deriving from a splitting of lateral visual cortical area.

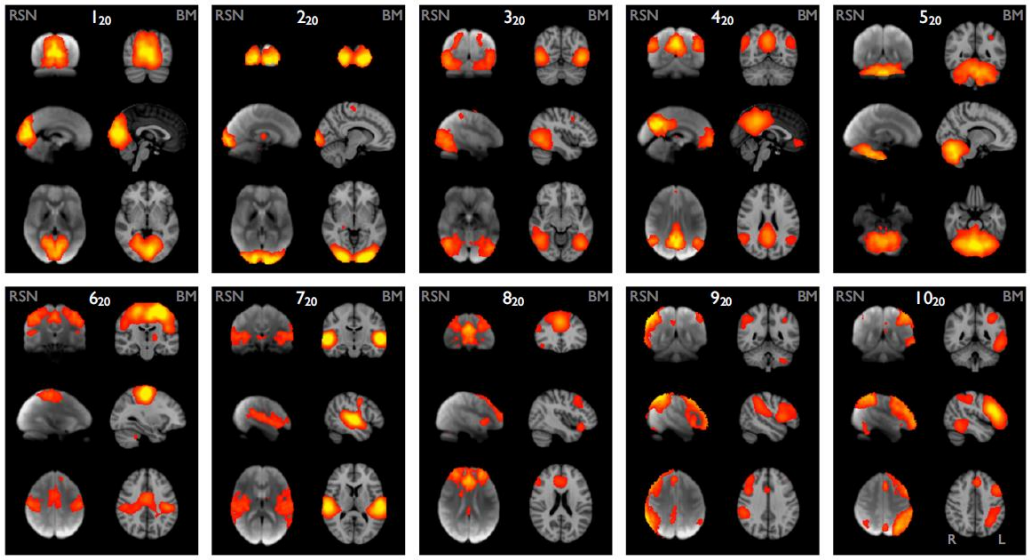

Figure 1.6. The 10 maps obtained by Smith and co-workers. in sagittal, coronal, and axial view. Left column of each pair corresponds to the resting fMRI data overlayed onto the mean fMRI image from all subjects. Right column of each pair corresponds to the network from specific task fMRI (Smith et al., 2009).

The networks identified are:

- Map 1_{20}: medial visual area.
- Map 2_{20}: occipital pole visual area.
- Map 3_{20}: lateral visual area.
- Map 4_{20}: default mode network (DMN) that correspond to the visuo-spatial system.
- Map 5_{20}: cerebellum (not identified in the study of Beckmann et al).
- Map 6_{20}: sensorimotor system
- Map 7_{20}: auditory system
- Map 8_{20}: executive control
- Map 9_{20}: frontoparietal right (correspond to the dorsal visual stream right)
- Map 10_{20}: frontoparietal left (correspond to the left visual stream left).

Each identified network is associated with a specific function and is located in a precise area of the brain (Beckmann et al. 2005; Smith et al., 2009):

- *Medial visual area* includes the medial posterior occipital cortex and the primary and secondary visual cortex. The corresponding Brodmann areas (BA) are 17-18-19. This network corresponds to the perception of vision and mainly to the visual stimuli in motion.
- *Occipital visual area* includes only the primary visual cortex (BA 17) and corresponds to the perception vision, mainly involved in the vision shape but also in the language and orthography cognition.
- *Lateral visual area* includes the temporal lobe of visual association (BA 37/39). The activation of these areas corresponds to a complex visualization, as the visual stimuli in motion, the perception of object shape in the visual field but also in the cognition space.
- *Default mode network* (or visuo-spatial system) includes the precuneus, the posterior cingulate, the medial parietal cortex, the bilateral inferior-lateral-parietal cortex and ventromedial frontal cortex. This network is the most widely studied RSN, since it is the most frequently seen as deactivating in task-based fMRI experiments; therefore, it is expecting

that this map does not correspond to any behavioural domain. Actually, the DMN is an interconnected and anatomically well-defined system, which is activated mainly when the subject is relaxed and not performing any task, not sleeping, and focused on imagining the future, remembering the past. This network seems strictly related to episodic memory.

- *Cerebellum* is involved in the equilibrium, in motor learning, and allows fine movement.
- *Sensorimotor system* includes the supplementary motor area (SMA), the sensorimotor cortex (motor cortex and primary somatosensory (SI)) and the secondary somatosensory cortex (SII). Basically, it includes the BA 4, 1, 2, 3 and 6. It corresponds to the action execution, the somesthesis perception, the bimanual movement and motor functions.
- *Auditory system* includes the primary auditory cortex and the auditory association. This network involves BA 41-42 (auditory cortex) and BA 21-22 (middle and superior temporal gyrus known as Wernicke area). This network corresponds to the auditory perception, but also corresponds to the speech elaboration and word processing (the speech can be understood), and to the word and speech execution, thanks to the involvement of the BA 22.
- *Executive control* includes the medial frontal cortex, the anterior cingulate and paracingulate gyri, and ventrolateral prefrontal cortex. This network corresponds to the action inhibition, and it is involved in the emotion cognition and in the somaesthetic perception of pain.
- *Frontoparietal right and left* include the frontal and parietal cortex. These networks are the only two strongly lateralized and correspond to:
    - Right: the somesthesis perception of pain (insular area) and the action inhibition.
    - Left: language cognition of orthography, phonology, semantics, speech, basically the verbal functions (thanks to the involvement of Wernicke and Broca area), but also correspond to working memory and executive functions.

1.4 Independent Component Analysis

There are numerous methodologies to study functional connectivity in the rs-fMRI data, aimed at detecting similarities across distinct regions of the brain. One of these methodologies is data-driven (or model-free) methods. It allows to examine whole-brain connectivity patterns, based on feature identification and extraction from data without requirement of prior assumptions. Importantly, this technique is commonly used in resting-state data since there is no predicted information about spatial and temporal patterns across the brain, so the resting-state design does not contain timing information that could justifies the underlying neuronal activity (Tianming et al., 2009).

Independent component analysis (ICA) is a kind of data-driven method and is adopted in a wide variety of fields. ICA was developed to allow the detection of unknown signals in a dataset, known as Blind Source Separation (BSS; Poldrack et al., 2011).

The observed BOLD signal (4D data) is a multivariate signal, resulting from a mixture of noise and signal of interest. To identify which signal represents noise and which represent neural activity, it is necessary to perform the unmixing of the observed BOLD signal. The aim of ICA is to decompose a multivariate signal into separate underlying components, which are statistically independent. Moreover, ICA is a linear model, so the original dataset can be recreated by summing all the components together (Bijsterbosch et al., 2017).

The ICA model is defined as

$$x = As$$

where x is the observed BOLD signal, s is a set of unknown sources and A is the unmixing matrix combining the components to obtain the observed signal (Poldrack et al., 2011).

The resulting component is described as a spatial map (which indicates the area in the brain where an activity is being detected) and a timeseries (which describes how the signal developed over time). Figure 1.7 shows a matrix representation of spatial ICA. On the left side 4D fMRI data contains the observed BOLD signal such that each row represents the 3D functional image at one time point and each column represents data from all time point at one voxel. The fMRI data set is

decomposed into two new matrices, the first one containing a time course of underlying signal in each column and the second matrix containing a spatial component's map in each row (Beckmann, 2012).

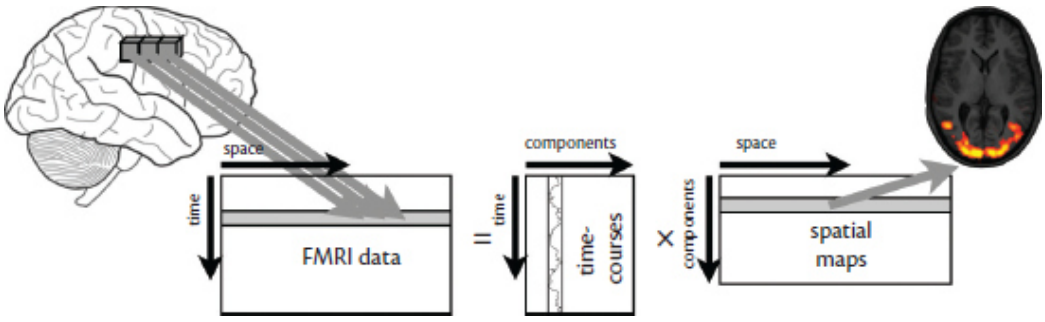

Figure 1.7. Schematic illustration of the data representation and the spatial decomposition performed by spatial ICA on fMRI data (Beckmann, 2012).

The ICA assumes that the components in *s* are statistically independent: this means that there is no statistical relationship between two derived components, in other words, there is no way to predict one signal based on knowledge of another signal (Bijsterbosch et al., 2017). The ICA uses the cost function to measure the statistical independence, which is optimized to find a good set of independent components (ICs). ICA is based also on the assumption that the source signal has a non-Gaussianity distribution. When signals are combined, the mixed signal has a Gaussian distribution, as shown in Figure 1.8. Therefore, to obtain a component that has a non-Gaussian source, i.e., the source is a signal and not a mixture of signal, it is necessary maximize the non-Gaussianity of sources. There are different functions, such as the negative entropy or Kurtosis (Bijsterbosch et al., 2017).

Not all the extracted IC are source of neural signal of interest, in that most are artefacts. The ICA has the capacity to separate neural-related signal from different sources of noise. For this reason, ICA is more and more frequently used in the context of data denoising (Griffanti et al., 2017).

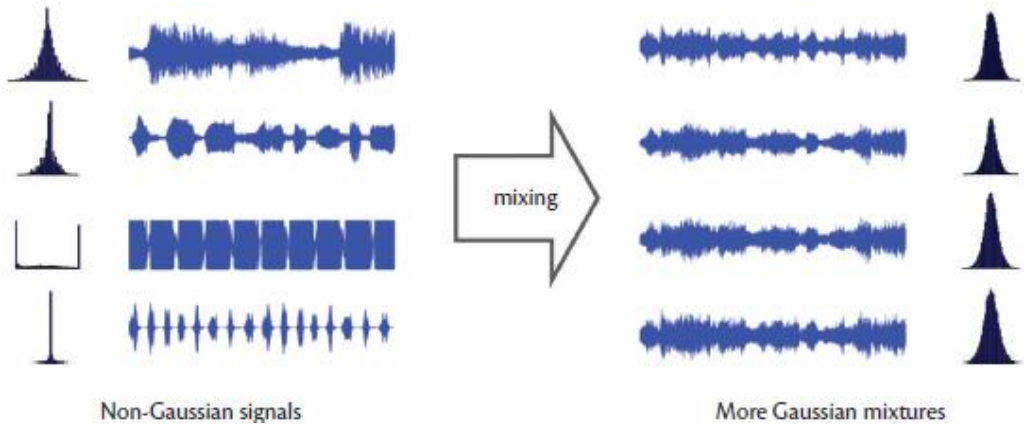

Figure 1.8. Mixing different non-Gaussian signals results in a more Gaussian signal (Bijsterbosch et al., 2017).

1.5 Aim of the study

The main purpose of this Thesis is to investigate the functional connectivity between the left and right hemisphere in a group of callosotomized patients, based on the analysis of resting-state fMRI data. In the literature there are conflicting results about the functional connectivity in these patients. Some studies affirm that the callosotomy reduces the interhemispheric functional connectivity (Roland et al., 2017). Others suggest the callosal resection would have no effect on the interhemispheric functional connectivity (Uddin et al., 2008). However, the first study was carried out on young epileptic patients (2-18 years old), who were followed up until 2 years after surgery; the second study reports data collected from a single old patient 4 decades after surgery. The patients on whom the present analysis has been performed are adult subjects, all of them but one operated in adult age, about two decades before the present study. For these reasons, the analysis of this particular group of patients, now quite rare in the world but still available at the University Hospital of Ancona, would allow to better understand the interhemispheric connections and the role of the CC.

To achieve this aim, the following specific objectives have been defined:

1. The analysis of functional and structural images was performed following a well-established methodology.
2. The evaluation of interhemispheric functional connectivity and the recognition of RSNs was performed by using the ICA analysis.

2. Materials and methods

This chapter describes the MRI acquisition parameters and the pre-processing performed to analyze the fMRI images applied to the six callosotomized subjects recruited for this study. In the final part, the denoising process using ICA is described. This thesis work was conducted in collaboration with the Department of "Scienze Cliniche Specialistiche ed Odontostomatologiche" of Università Politecnica delle Marche and the Riuniti Hospital of Ancona.

2.1 Participants

Data used in this thesis were acquired from six right-handed patients, P1, P2, P3, P4, P5, P6 (age: 30-60 years; M/F = 4/2) who had severe epilepsy episodes in their history. Except for P5, the other patients underwent callosotomy surgery different years ago. Specifically, P1, P2, P4, P6 underwent complete forebrain callosotomy whereas a portion of CC was not cut in P3's callosotomy surgery. MRI data acquisitions were performed between May 2018- June 2019. The clinical patient's details are reported in Table 1.

Table 1. Clinical details of patients.

Case	Gender	Age at testing	Handedness (Oldfield score)	Callosotomy	Years after 2nd surgery
P1	M	42	Right (21)	Total	23
P2	M	52	Right (10)	Total	24
P3	M	60	Right (10)	Partial posterior	19
P4	F	46	Right (10)	Total	19
P5	F	30	Right (10)	No surgery	
P6	M	46	Right (10)	Total	24

2.2 MRI data acquisition

During the resting-state fMRI acquisition, the subjects were instructed to lie down and stay still as much as possible, to keep their eyes open, to relax without falling asleep and without focusing on anything.
Resting-state BOLD fMRI data and T1-weighted structural images were acquired using a 1.5 Signa HDxt GE Medical System MRI scanner.
A gradient-echo EPI sequence was used to acquire the functional images with parameters TE= 50 ms, TR= 3000 ms, flip angle= 90°, FOV of 192 × 192 mm, matrix size of 64 × 64, number of volumes= 300, number of axial slices= 35, slice thickness= 4 mm with no gap between slice acquisition and voxel resolution is 3×3×4 mm. The duration of RS-fMRI was 900 s (15 minutes).

For anatomical localization and for coregistration with 3D data set, a T1-weighted structural image (high-resolution whole-brain images) was acquired using a MPRAGE sequence with parameters TE= 6.7 ms, TR= 14.7 ms, FOV of 256×256 mm, matrix size of 512×512 mm, number of sagittal slices= 158 (166 in the RM data acquisition), slice thickness is 1 mm with no gap between slice acquisition and the voxel resolution is 0.5664×0.5664×1 mm.

2.3 Pre-processing

After data acquisition, the structural and functional MRI images were processed using dedicated software in order to obtain the information necessary for the subsequent ICA analysis.
The software used in this work were two:

- *FSL (FMRIB Software Library;* Smith et al., 2004) is a software created by the Analysis Group, FMRIB, Oxford, UK, FSL, and is a comprehensive library, open-source, analysis tools for fMRI, MRI and DTI Brain Imaging data. It works on Apple and Linux (Windows 10 via a virtual machine). Most of the tools can be run either from the command line in the case of Linux from the shell

or as a GUI (Graphical User Interfaces). By default, FSL uses the Nifti_GZ image format, i.e. the compressed NIfTI file (.nii or .nii.gz). When MRI brain images are acquired, they are DICOM images. It is necessary to convert them to the NIfTI format, which is considered the new standard format for medical images. At this purpose, in addition to FSL software, it was also MRIcron software to convert the DICOM file into a Nifti file (*https://www.nitrc.org/projects/mricron*).

- *BrainVoyager (BV; v2.4;* Formisano et al., 2005) is a powerful neuroimaging software package for data management and data analysis. It is a tool for the analysis of anatomical and functional MRI data sets, and also for the DTI data. The software is available and running on all major computer platforms included Windows 10.

Prior to fMRI statistical analysis, there are multiple important steps to be performed in order to eliminate artefacts and noise components in fMRI. A series of pre-processing pipelines are typically used on raw data and the standard operations are mentioned in Figure 2.1. At each step, quality control must be assured to verify effectiveness of the pre-process technique as well as prevent error propagation (Poldrack et al., 2011).

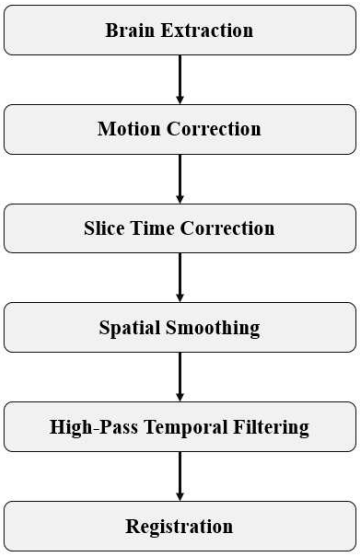

Figure 2.1. Common fMRI pre-processing steps.

For each fMRI dataset, the following steps were executed when using both the softwares. In the case of FSL, it was used MELODIC tool, by selecting MELODIC ICA GUI or by typing Melodic_gui on the shell (Smith et al., 2004).

2.3.1 Brain extraction

The first pre-processing step was performed on the T1-weighted structural image, to differentiate brain tissue from non-brain tissue. In the structural images, both brain and non-brain tissue are visible (the skull, eyes, neck). The robustness of the registration increases if these parts of non-brain tissue are removed before the registration step is performed.

- *FSL*: the non-brain tissues were removed from the structural image by using BET, the Brain Extraction Tool of FSL, Figure 2.2 (Jenkinson et al., 2005). This algorithm is completely automated; furthermore, since each image of the brain is different, there are some parameters that can be adjusted to obtain a better result, such as the fractional intensity threshold parameter (-f option on the command line). This parameter controls the threshold that distinguishes brain from non-brain tissue. Although BET generally does a good job in extracting the brain, it may happen that some portions of non-brain tissue are not removed properly; however, it is preferable to preserve the non-brain tissue rather than remove portions of the brain (Jenkinson et al., 2005). This extracted brain is renamed "_brain" and is the structural image used as "highres" image in the registration step.
- *BV*: to improve the quality of the anatomical data set, the automatic intensity inhomogeneity correction tool (auto-IIHC) is used (Figure 2.3). It is an automatic method which includes 4 steps: background cleaning, brain extraction, white matter detection and bias field estimation within white matter voxels (Goebel et al., 2011).

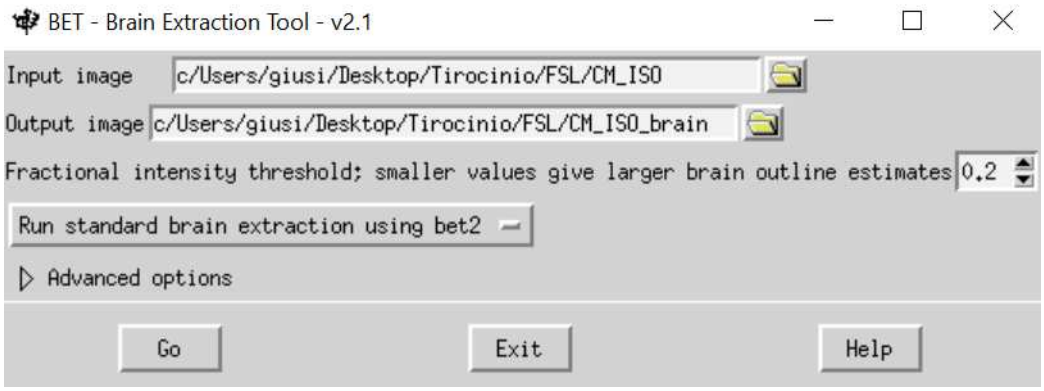

Figure 2.2. Brain Extraction Tool of FSL software.

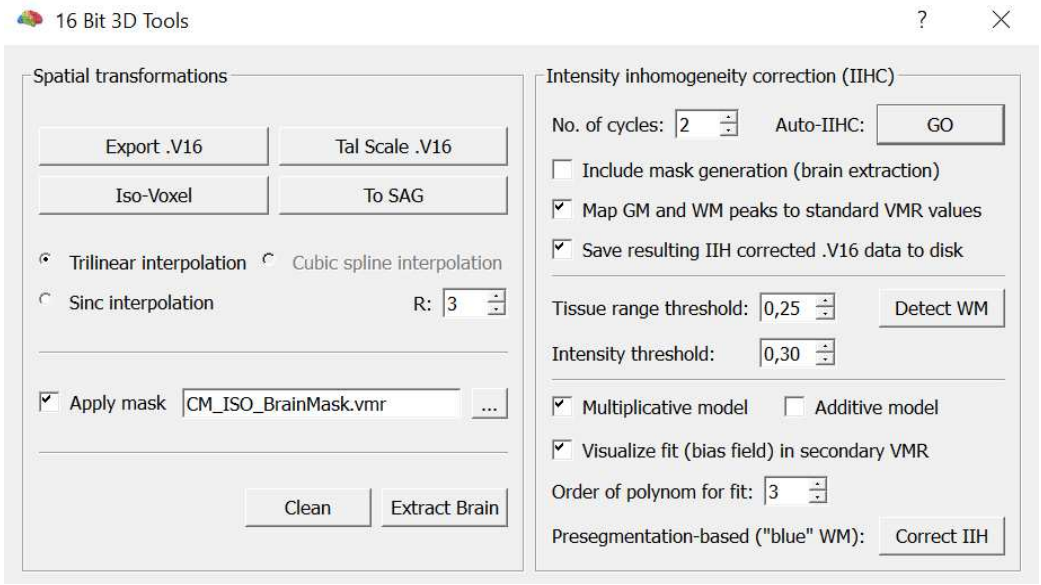

Figure 2.3. Intensity Inhomogeneity correction tool to brain extraction in BrainVoyager software.

2.3.2 Data selection

Before to perform the pre-processing steps, such as motion correction, slice time correction, spatial smoothing and temporal filtering, it is necessary select the fMRI data.

- *FSL*: In the "Data" section, was selected the 4D data (fMRI file in -nii.gz format) and the first 2 volumes have been deleted before any processing.

- *BV*: by creating a new FMR project, the DICOM file were selected, and the number of volumes and slices were set. Also, in this case the first 2 volumes have benne deleted.

2.3.3 Pre-statistical analysis

As described in the figure 2.1, before the co-registration there are some main steps to be performed, corresponding to the pre-processing of fMRI data, to the correction of the head movement, filtering the noise and smoothing the fMRI images. The pre-processing used on the data set is the same for both software. In the Figure 2.4 the pre-stats performed on FSL is showed, and in the Figure 2.5 the pre-processing performed by using BV is showed.

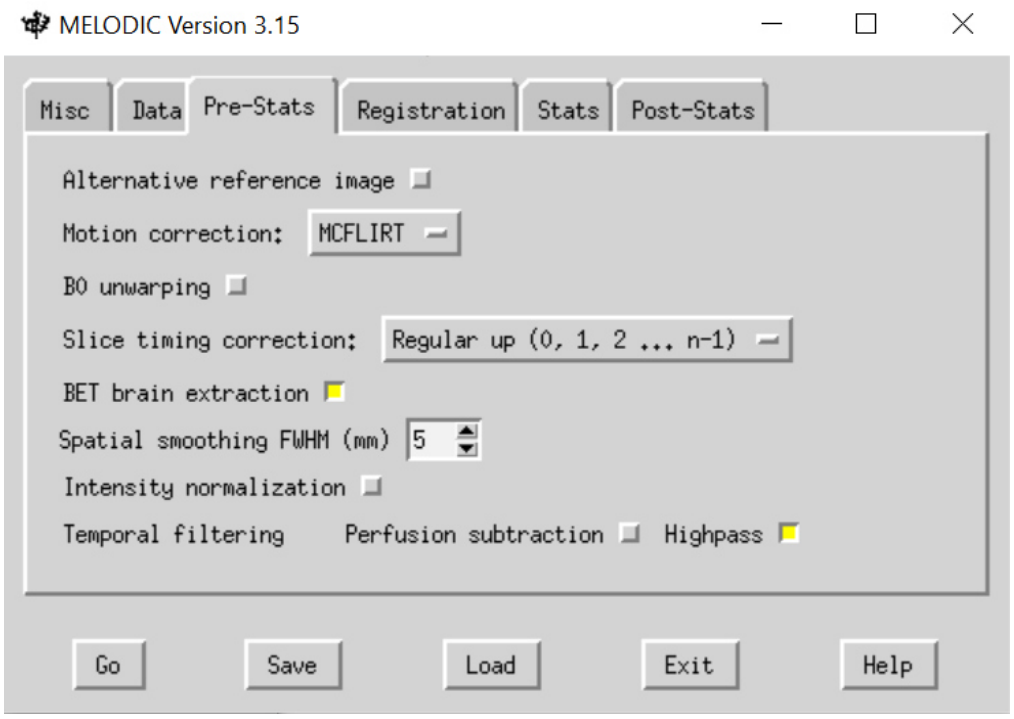

Figure 2.4. The pre-processing steps selected in the MELODIC GUI of FSL.

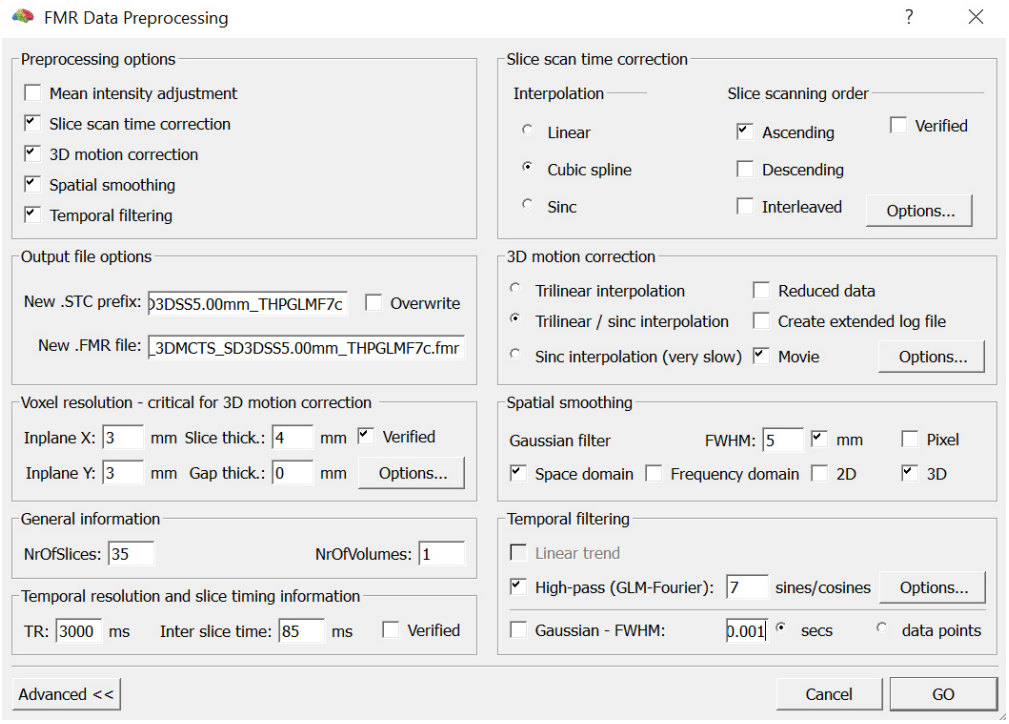

Figure 2.5. The pre-processing steps selected in the BrainVoyager software.

2.3.3.1 Motion correction

Head movement correction is the main pre-processing procedure. Motion correction, also known as realignment, is an important issue in the analysis of fMRI data since even the smallest movement of the patient can induce significant artifacts (also of a greater intensity than the BOLD signal). Displacements of the subject's head, by the fraction of a millimetre, can generate variations in the signal greater than 2%. Such artifacts are common at the edge of the brain or near large vessels. Subjects' head motion can result in a misalignment of successive slices leading to incorrect anatomical positions between voxels of subsequent images. There are different systems of head immobilization, however, they are often not sufficient to completely eliminate movement (especially the involuntary one). The need to realign the images to a common reference is because during data analysis, at each time point the time series corresponding to a specific voxel is supposed to belong to the same brain area.
The standard method of correction describes the movements of the head through 6 parameters, 3 of translation (x, y, z) and 3 of rotation (roll, pitch, yaw),

designed to characterize the motion of rigid bodies in 3D space. This means that each image can be moved without brain deformation (Jezzerd et al., 2001).

- *FSL:* the motion correction procedure was developed based on an affine registration tool in FSL called MCFLIRT (Jenkinson et al., 2002). MCFLIRT operates by choosing a functional volume of the acquisition as the reference volume, to which all other volumes will be aligned. An iteration mechanism is performed during which each volume is aligned with a common reference (e.g., one original volume, mean of several images or a standard space image), by minimization of a cost function (Smith et al., 2004).
- *BV:* in the "Analysis" menu select "FMR Data Preprocessing" and it was selected "3D motion correction". All the other values have been left by default (Formisano et al., 2005).

2.3.3.2 Slice time correction

Functional MRI acquisitions uses two-dimensional techniques. This means that fMRI sequences do not acquire each slice in a volume at the same time and therefore the slices have different acquisition times. Slices can be acquired sequentially (ascending or descending order) or in an interleaved way. Slice timing problems may severely prejudice the analysis since fMRI analysis is based on the signal time course. In this way, slice timing correction methods attempt to fit the problem of slice acquisition delays. The most regular strategy is data shifting, according to which voxel's time series is shifted according to a reference slice through interpolation, so that all slices match in time. However, this technique generates blurring and data degradation that can propagate through the different slices (Bijsterbosch et al., 2017).

- *FSL*: Since the subjects' fMRI sequences were acquired sequentially in the ascending order (from the bottom to the top), was chosen Regular up in the pre-stats section.

- *BV*: in the "FMR Data Preprocessing" was selected Slice time correction and the cubic spline was chosen as interpolation function, with ascending order.

2.3.3.3 Spatial smoothing

In most fMRI studies, spatial smoothing is commonly applied, and consists of the averaging of neighbouring voxels. A filter is applied to the image to remove the highest frequencies from the frequency domain, prevailing low-frequency information typical of neural activity at rest. Consequently, smoothing improves signal-to-noise ratio (SNR) at the cost of loss in spatial resolution (the higher the filter the blurrier the image), as shown in Figure 2.6. Through blurring, the large variability across individuals is diminished, thus providing better registration results. However, partial volume artefact may occur because brain voxels can be averaged with non-brain tissue/background, resulting in inaccurate signal intensity. Additionally, smoothing may eliminate significant functional activations, or can cause regions that are functionally different to combine with each other (Poldrack et al., 2011).

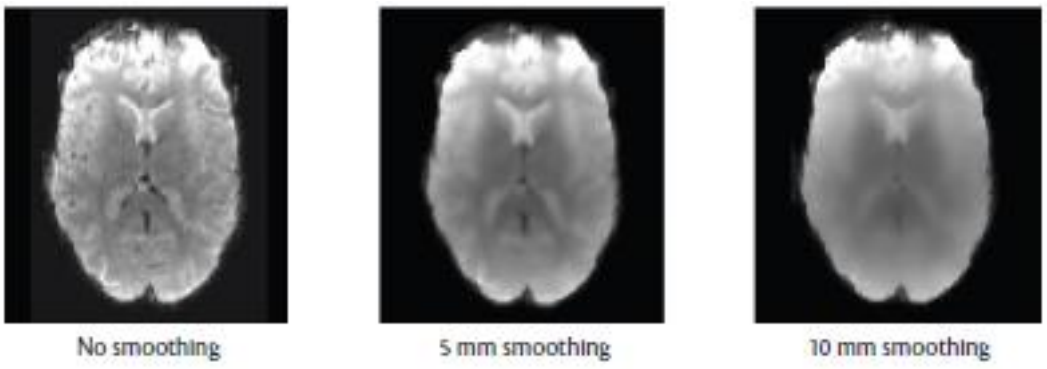

Figure 2.6. The effect of the spatial smoothing on the image. The higher the filter, the blurrier is the image (Bijsterbosch et al., 2017).

Smoothing involves the convolution of the fMRI image with a three-dimensional Gaussian kernel, that is a filter, which is determined by the full width at half maximum (FWHM) parameter, or in statistical terms, the standard deviation. FWHM is the diameter of the smoothing kernel at half of its height. A larger

value of FWHM represents greater data smoothing, as shown in Figure 2.7 (Bijsterbosch et al., 2017).

When this pre-process tool is used, the correspondent smoothness is given by

$$FWHM = \sqrt{FWHM_{intrinsic}^2 + FWHM_{applied}^2}$$

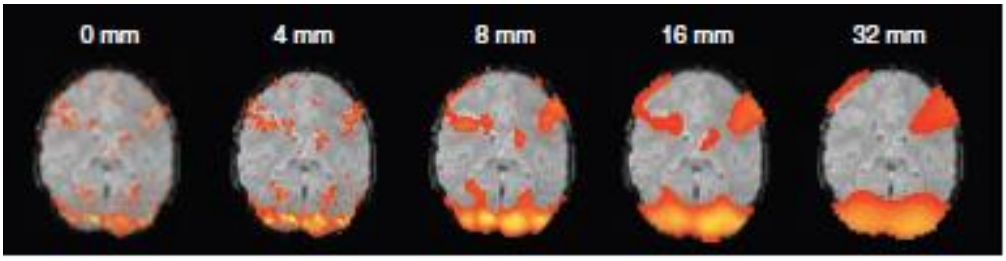

Figure 2.7. A large value of FWHM show an activity in more voxel, leading to greater detection of large cluster but decreased detection of smaller cluster (Poldrack et al., 2011).

The quantity of smoothing should be the minimum to achieve a given result and it depends on the type of study that is being conducted. Roughly, the recommended amount of smoothing is the double of voxel dimensions (Poldrack et al., 2011).

In both FSL and BV software a FWHM = 5 mm was used.

2.3.3.4 Temporal filtering

Temporal filtering is the last pre-processing step, used to remove the unwanted signal components from the time-series of each voxel, without removing the signal of interest. Essentially, fMRI data is high-pass filtered, which means that the lowest frequencies are removed from the data (ideally lower than the low-frequency fluctuations typical of the BOLD signal). The amount of temporal filtering applied is expressed using a cut-off frequency (expressed in Hertz) or cut-off period (expressed in seconds) and depends on the data quality. For high quality datasets it is possible to set a higher cut-off frequency (0.001 Hz) in order to remove less and retain more data, whereas lower quality datasets often use lower cut-off frequency (0.01 Hz) in order to remove more noise (Bijsterbosch et al., 2017). In both FSL and BV software a high-pass filter with a cut-off

frequency of 0.01 Hz was used, so that any signal fluctuations that vary more slowly than the cut-off frequency value will be (entirely or partially) removed.

2.3.4 Registration

The last step before the statistical analysis is the registration. Since in the fMRI studies were acquired both the functional images (during the execution of a task or in resting state) and the T1-weighted structural image of the same subject, the registration is crucial to have a voxel-anatomical correspondence between them. The structural image has a higher spatial resolution than the functional image that derives from the BOLD signal. To delimit and precisely recognize the regions of interest within the functional image, in order to interpret the results and understand in which brain regions the voxels are active, it is necessary to align the functional image with the T1-weighted structural image of the respective subject. Both the functional and structural images of the subject are in the native space in which the data are acquired. Because the human brain differs from one subject to another both in size and shape, it is needed to align the functional and anatomical images of the subject with the standard space to perform a comparison between different subjects, in order to make the results more easily integrated and comparable (Figure 2.8).

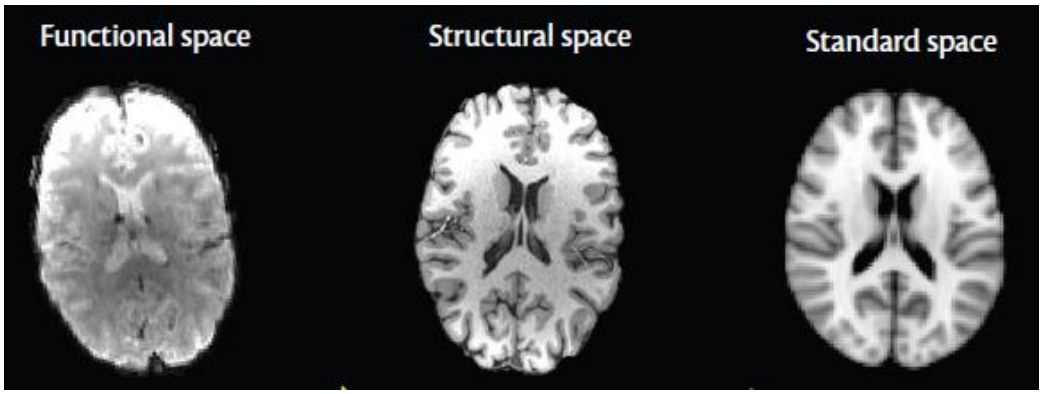

Figure 2.8. Registration methods are used to align the subject's functional and structural image (both in native space) into the same standard space (Bijsterbosch et al., 2017).

All acquisitions can be aligned to a specific template, which is an image that is representative of the atlas (a guide to localize the activation and interpret the

result) and provides a target to which individual images can be aligned (Poldrack et al., 2011).

The standard space is a common coordinate system and the widely used atlases are:

- the *Talairach atlas*, created by Jean Talairach (Talairach and Turnoux, 1988). It is based on the post-mortem brain of a 60-year-old woman, and it has a precise anatomical location. He proposed a "three-dimensional proportional grid", which is based on a set of anatomical landmarks: the anterior commissure (AC), the posterior commissure (PC), the midline sagittal plane, and the exterior boundaries of the brain at each edge. Given these landmarks, the origin (zero-point) in the three-dimensional space is defined as the point where the AC intersects the midline sagittal plane. The axial plane is then defined as the plane along the AC/PC line that is orthogonal to the midline sagittal plane, and the coronal plane is defined as the plane that is orthogonal to the sagittal and axial planes. In addition, the space has a *bounding box* that specifies the extent of the space in each dimension, which is defined by the most extreme portions of the brain in each direction, as shown in Figure 2.9 (Poldrack et al., 2011).

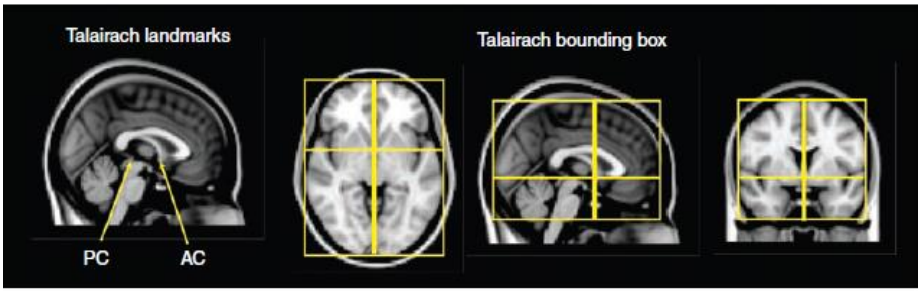

Figure 2.9. Talairach space is defined by a number of landmark. On the left are identified the anterior commissure (AC) and the posterior commissure (PC). On the right is determined the bounding box for Talairach space (Poldrack et al., 2011).

- the *Montreal Neurological Institute (MNI)* atlas, and the most famous is the MNI152 (Figure 2.10), based on the calculation of a non-linear average of 152 brains of normal control subjects (all right-handed).

The MNI152 atlas is slightly larger (in particular 5 mm taller, 5 mm longer and 10 mm deeper (Lancaster et al., 2017) and less precise than that of Talairach but is the most used. The registration to the Talairach template requires the identification of anatomical landmarks, and this kind of method has generally been rejected in favour of automated registration to image-based template, such as MNI152 (Poldrack et al., 2011).

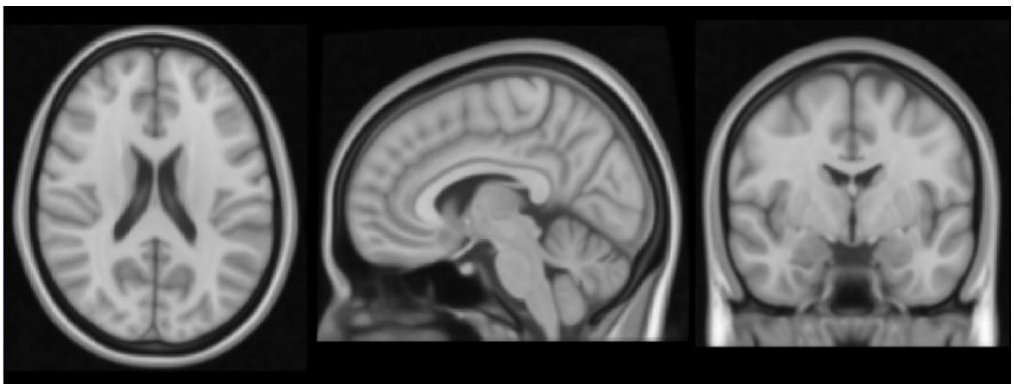

Figure 2.10. MNI152 template on FSLeyes.

To convert the MNI coordinates in Talairach coordinates, a MATLAB function (Lancaster et al., 2017) or an automatic algorithm (https://bioimagesuiteweb.github.io/webapp/mni2tal.html) could be used, but the result provides not a very good match due to the difference in brain shape.

The registration is a two-step process:

1. In the co-registration step, the realignment of the pre-processed functional images on the corresponding T1-weighted anatomical image (-weighted) is carried out. The goal is to superimpose the information contained in the functional images on an image where it is possible to discriminate between the anatomical regions.
2. The second step is known as normalization and consists of the registration of the subject's image (both functional and anatomical) to

the atlas. The main advantages derive from the possibility to generalize the results to a larger population of subjects, to improve the comparison between different studies and conduct an averaging process between the various subjects.

By performing this procedure for each functional volume, the registration of all images functional to the standard space is performed.

- *FSL* (Figure 2.11)
    1. The first step is the co-registration of the reference functional image to the high-resolution structural brain image, obtained from the BET (called "main structural image"), through the boundary-based registration (BBR) method, which is cost function that measure the goodness of alignment by looking for white-matter boundaries in the fMRI image since considerable differences across these boundaries are expected (Greve and Fischl, 2009).
    2. The second step is the normalization. First, it is used the linear registration to register the high-resolution structural brain image to a standard space (MNI152, T1-weighted, 2×2×2 mm) with resampling resolution at 4 mm. It was used FLIRT and 12 degrees-of-freedom (3 translations, 3 rotations, 3 zooms, and 3 shears; Jenkinson et al., 2002). The linear registration is used in order to initialize the non-linear registration and is performed using FSL's tool FNIRT (Andersson et al., 2010), which enables better alignment of internal structures. Non-linear transformation is used after linear transformation for optimal accuracy. The cost function used in FLIRT is the correlation ratio, whereas in FNIRT the function is the sum-of-squares difference and the displacement fields for each dimension are applied. The warp resolution was set to 10 mm.

3. Finally, the two transformations are combined, taking the low-resolution fMRI image into the standard space.

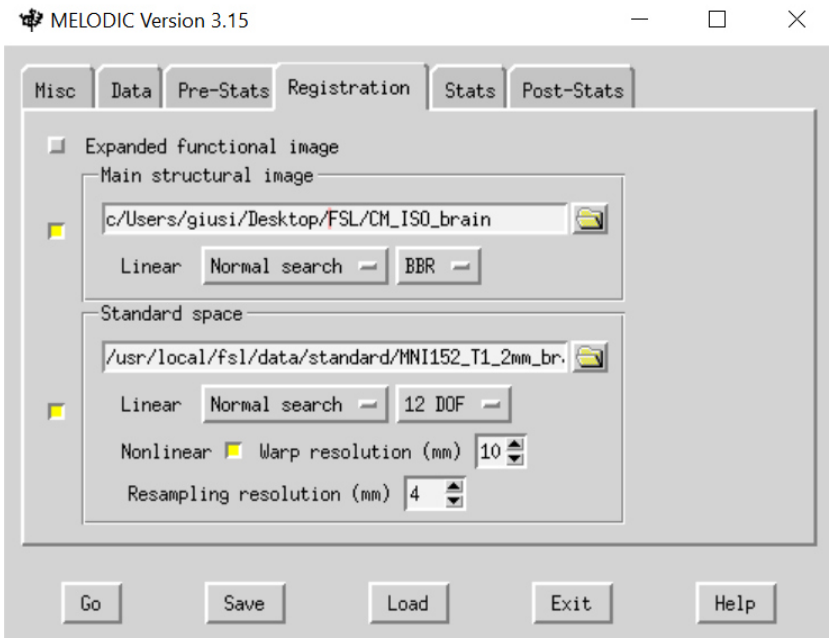

Figure 2.11. Registration step by using FSL software.

- *BV* (Figure 2.12 and Figure 2.13)
    1. The first step is the co-registration of functional images (FMR) and the structural image (VMR). By opening the "3D Volume Tools" in the co-registration section, the pre-processed functional file was selected and aligned with the structural file, by running both the Initial Alignment and Fine-Tuning Alignment (Figure 2.12).
    2. The second step is the normalization. The structural data are transformed into Talairach space. Since the CC was resected in most subjects, the automatic transformation is not usable, therefore it was necessary to identify the points in a manual way. First, the AC was identified, then the PC and the AC-PC plane, and finally the other landmark points, such as AP (the most anterior point of the cerebrum), PP (the most posterior point), SP (the superior point), IP (the inferior point), RP (the most right point) and LP (the most left point; Goebel et al., 2011).

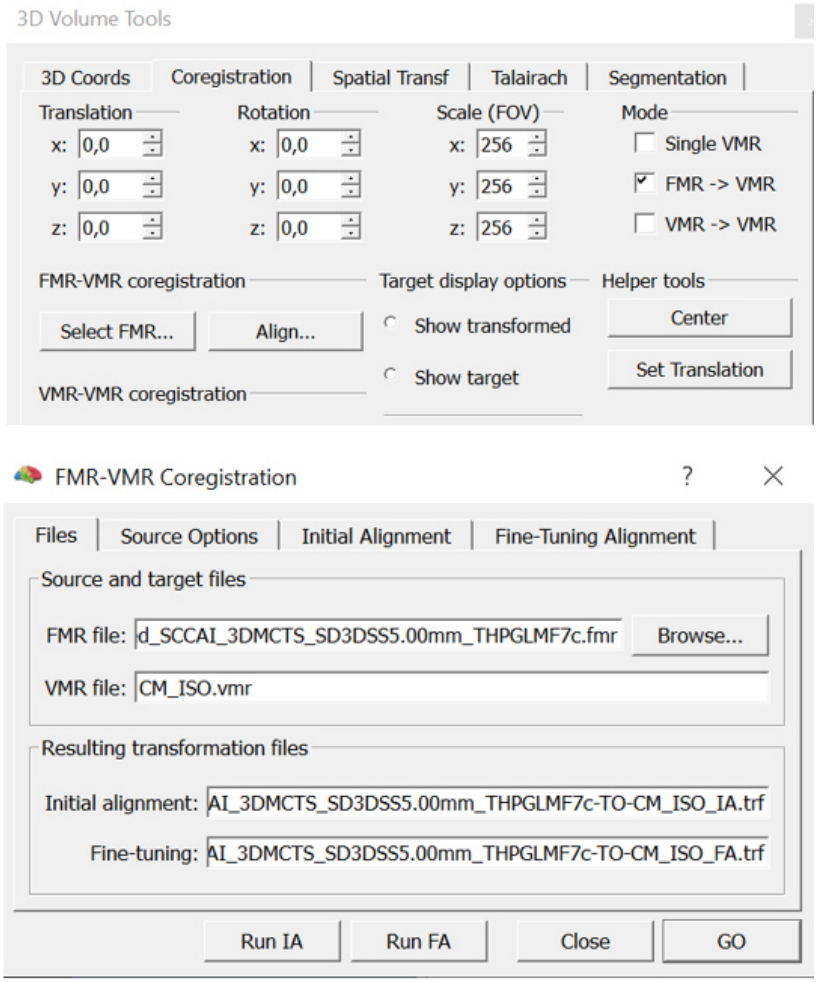

Figure 2.12. Coregistration between the fMRI and the structural file.

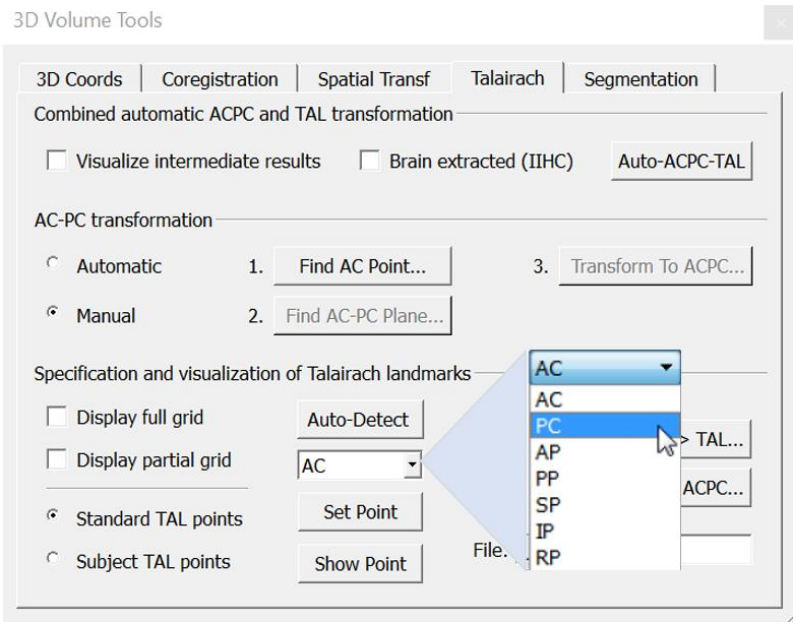

Figure 2.13. The structural ISO file is registered into Talairach space.

2.4 Independent Component Analysis

2.4.1 FSL

Functional MRI data consist of the neural signal of interest, but also of noise signal. Although a pre-processing of fMRI data is applied, some structured noise could remain. The aim of ICA decomposition is to separate the data into non-Gaussian sources to improve the specificity and sensitivity of results derived from observed BOLD signal.

However, ICA does not have the ability to quantify statistical significance for estimated spatial maps; in addition, ICA is "noise-free", that means it does not include the noise/error term added to the source, causing the problem of overfitting the components. Beckmann and Smith proposed a probabilistic ICA (PICA) model for fMRI data and this new methodology is implemented in MELODIC software in FSL (Beckmann and Smith, 2004).

The PICA model includes a noise term

$$x = As + e$$

where e~$N(0, \sigma)$. The model has improved by adding other processes, such as the voxel-wise temporal prewhitening, the variance normalization of time series, and the use of a prior information about the spatiotemporal nature of source processes. Then, the obtained spatial maps are transformed in Z-scores, and therefore it is necessary to decide an appropriate threshold value (usually is |Z|>2.0), above which the value of Z correspond to statistically significant activations with respect to the background noise. In order to perform an inference and then evaluate the maps in relation to the voxels activated in a significant way, the PICA algorithm uses the probabilistic mixture modelling model applied to the probability density of the Z-scores spatial maps. The distribution of statistical data of interest was divided into two components, one for the non-activated voxels and one for the activated voxels. In MELODIC software the Gaussian/Gamma Mixture Model (GGM), shown in Figure 2.14, is implemented. This approach allows to model the histogram of inactive voxel (Gaussian background noise) with a Gaussian distribution (dominantly models the intensity histogram), whereas the histogram of the Z maps of the non-

Gaussian source (activated voxel) with gamma distributions (both negative and positive gamma; Beckmann and Smith, 2004).

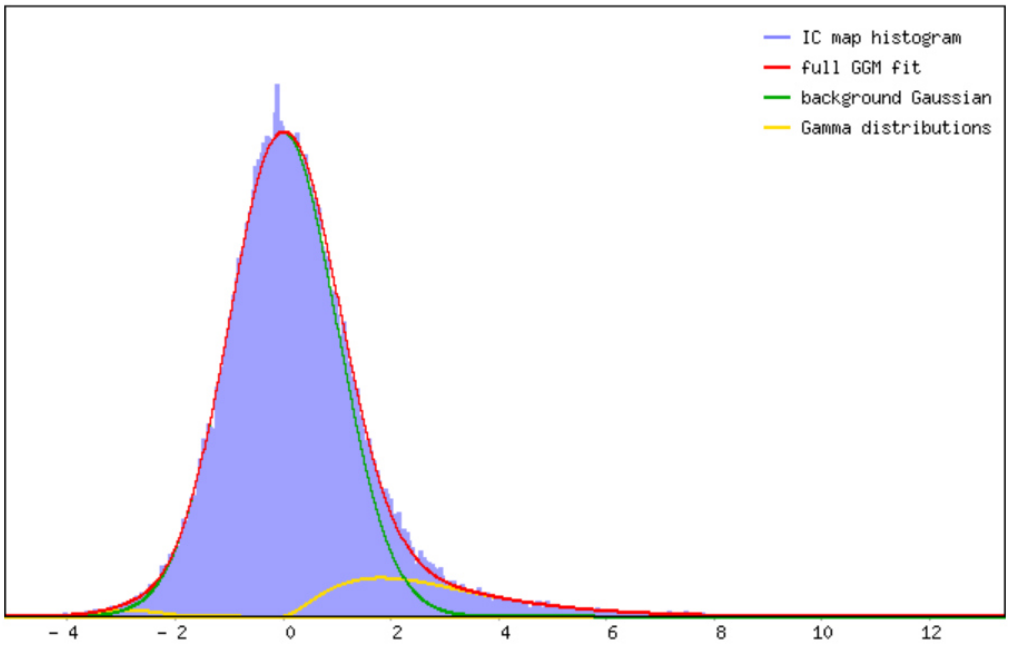

Figure 2.14. Gaussian/Gamma Mixture Model implemented within FSL used to model the histogram of inactive voxel with the Gaussian distribution (green curve) and the active voxel with Gamma distribution (yellow curve; Beckmann, 2012).

Figure 2.15 shows a schematic representation of PICA methods implemented in MELODIC, which results in a PICA map that shows the active voxel with a statistical significance. The activated voxel does not mean a neural activity of interest, in that the activation might also be an artefact.

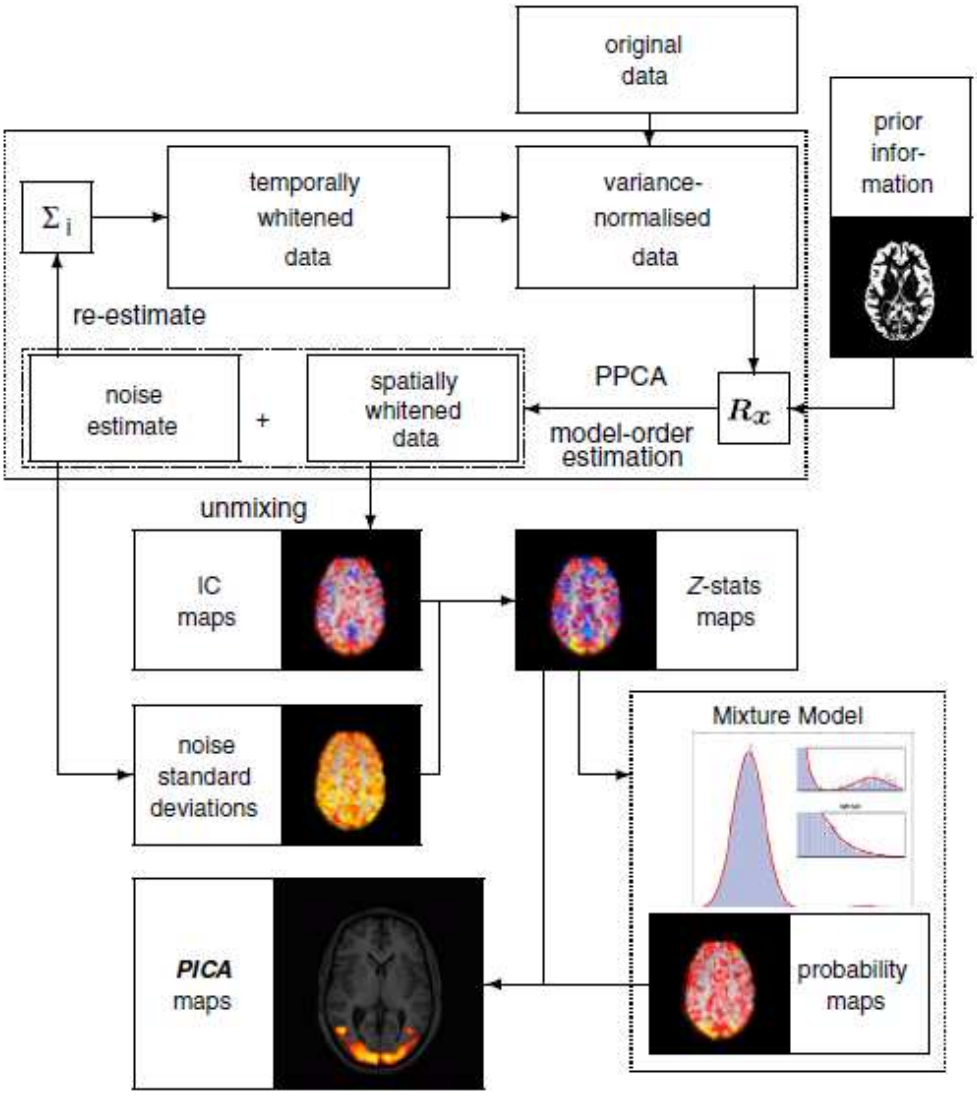

Figure 2.15. A schematic illustration of the probabilistic ICA (Beckmann, 2004).

As mentioned above, the MELODIC tool of FSL implemented the PICA method. Figure 2.16 shows the selected option to perform the single subject analysis. The number of IC are estimated in automatic way and the value chosen as threshold to identify the activated voxel was p>0.5.

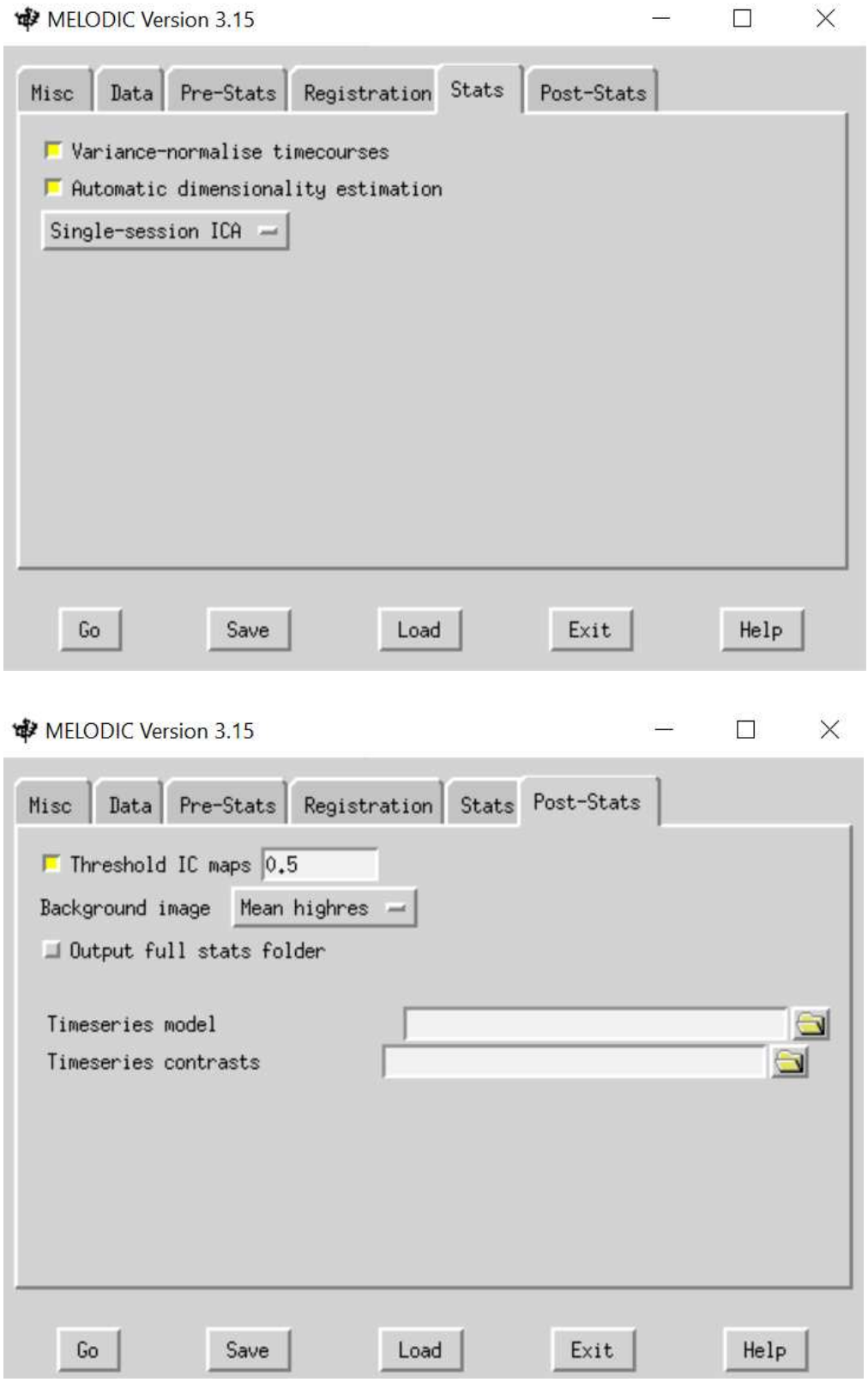

Figure 2.16. A single subject statistical analysis performed by using MELODIC tool.

2.4.2 BrainVoyager

In BV, the spatial decomposition of the data is performed using "FastICA". In this case, a fixed-point ICA algorithm minimizes the mutual information of the components using a robust approximation of the negentropy as a contrast function and a fast, iterative algorithm for its maximization. Before applying spatial ICA, the temporal dimension of the data set may be optionally reduced using Principal Component Analysis (PCA; Formisano et al., 2005).

To run FastICa it was used the deflation approach and Gaussian as Nonlinearity function. The number of components was by default kept 30 (Figure 2.17).

The input file to perform the spatial ICA is a VTC (volume time course) data set. The threshold value was 10 and Z>2.

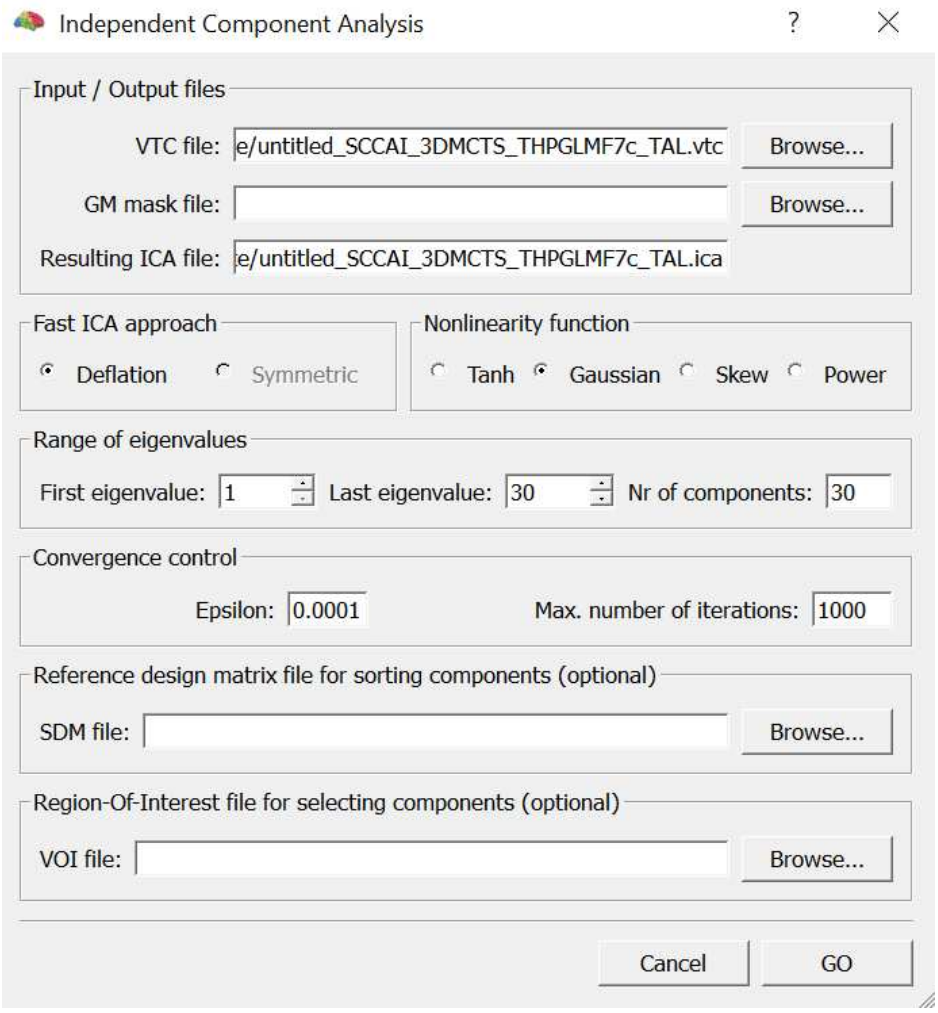

Figure 2.17. ICA illustration of BrainVoyager software.

The original fMRI data was pre-processed to improve the quality of data and then transformed into a normalized 3D space, known as VTC file. The VTC file was linked with the subject's normalized anatomical file. This allows to perform the ICA on a group of subject and compare the IC across the subjects.

2.4.3 Hand Classification of Independent Components

ICA produces many different spatiotemporal components, and the information represented in the ICA decomposition is used to recognize the noise independent components (N-ICs), i.e. the components characterized by a noise/artefact signal, and the neural signals independent components (S-ICs), which represent the signals of interest. N-ICs and S-ICs differ in terms of spatial, temporal and spectral characteristics. This helps to reduce the negative effect of noise on the analysis of fMRI data. Different approaches have been described to label the components, most of which are fully automated, particularly useful when dealing with a large population of healthy subjects. In the case of small sample size with unusual characteristics, such as Alzheimer's or epileptic patients, it is preferable to use a visual inspection of the components, which is the gold standard technique but besides being time-consuming, the manual labelling requires expertise (Griffanti et al., 2017).

The aim of ICA-based data clean-up is to maintain as much signal as possible, by removing artefacts from the fMRI data, and its success depends on the accuracy of labelling the ICs (Robert et al., 2010).

To classify a component, it is necessary to inspect for each component:

- *the spatial map*, which observes the number and dimension of clusters of active area, if the clusters overlap the grey matter (GM) or overlap the blood vessels, cerebrospinal fluid (CSF), white matter (WM) or the edge of the brain. It is a major piece of information to discriminate signal of interest from noise (Griffanti et al., 2017).

- *the time series*, which checks the overall aspect, if there are one or more sudden peaks or if it shows a saw-tooth pattern (regular alternation of up and down) (Robert et al., 2010).
- *the power spectrum*, which checks where the distribution of power in the frequency domain occurs, if at low frequency or at high frequency (Robert et al., 2010; Griffanti et al., 2017).

The features to identify a component are summarised in Table 2 (Griffanti et al., 2017). Specifically, the S-IC should have a low number of large clusters localized in the GM (note that if the data have been smoothed, the clusters will have a larger area than the non-smoothed data). Moreover, the clusters continue across slices, following the GM ribbon in all views. The time series should have a saw-tooth pattern, and the power spectrum plot should have a predominantly low-frequency value, with a peak between 0.01 - 0.1 Hz, to indicate the movement of oxygenated blood. An example of S-IC is shown in Figure 2.18.

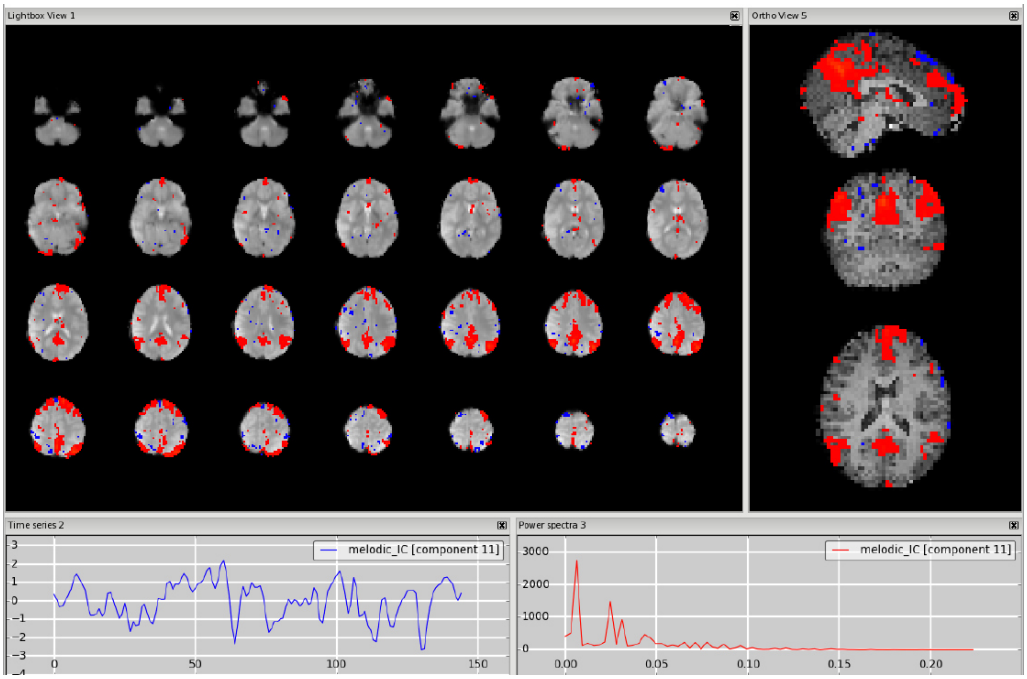

Figure 2.18. An example of signal component showing the Default Mode Network. The time series does not contain sudden jumps and the power spectrum is predominantly low frequency (Griffanti et al., 2017).

Table 2. Features of signal and noise independent components

Features	S-IC characteristic	N-IC characteristic
Spatial		
Number and dimension of clusters	Low number of large clusters	Large number of small clusters
Overlap with GM	Clusters' peaks in GM and overall good overlap of the clusters with GM.	Indiscriminate overlap with non-GM tissues, or clusters' peaks in WM/CSF
Overlap with WM, CSF, blood vessels	Very low or absent overlap with WM, CSF, blood vessels	High overlap with one or more of WM, CSF, blood vessels
Overlap with brain boundaries or areas close to the edges of the FOV.	Very low or absent overlap with brain boundaries. Clusters follow known anatomical (e.g. structural/ histological) boundaries.	Ring-like or crescent shape or stripes near the edges of the field-of-view
Location near area of susceptibility induced signal loss (e.g. orbitofrontal)	Generally located away from these areas	Located within the region of signal loss (e.g. areas of air-tissue interface)
Non-biological, acquisition-related patterns	Patterns have no relation to acquisition parameters	Often show banding patterns in slice direction or streaks along the phase encoding direction, accelerated sequences may have centrally located artefacts
Temporal (and spectral) features		
Overall aspect of the time series	Fairly regular/oscillatory time course	Large jumps and/or sudden change of oscillation pattern.
Distribution of power in frequency domain	Predominantly low frequency (at least one strong peak within 0.01 – 0.1 Hz)	Predominantly high frequency, very low frequency, or pan frequency

Consequently, the components are classified as N-IC if in the spatial maps they show isolated clusters across slices, or many small clusters localized on the blood vessels, WM, CSF, or at the edge of the brain; if the time series is characterized by large jumps and/or one or more sudden peaks, and if they have a predominantly high frequency or very low frequency (<0.01 Hz) distribution.

The common artefact identified in the study of Griffanti and coworkers (Griffanti et al., 2017) are:

❖ Motion artefact (Figure 2.19): it manifests in the spatial maps as a ring of activation around the edge of the brain and in the time series plot as a sudden spike (in correspondence to sudden peak in the motion correction graphic derived from the pre-processing). The cause of this artefact is the movement of head during the acquisition. In the case of head translation, the ring may be more visible on the axial plane, whereas head rotation will result in a ring visible on the sagittal plane. For this reason, it is necessary to inspect every single slice and plane.

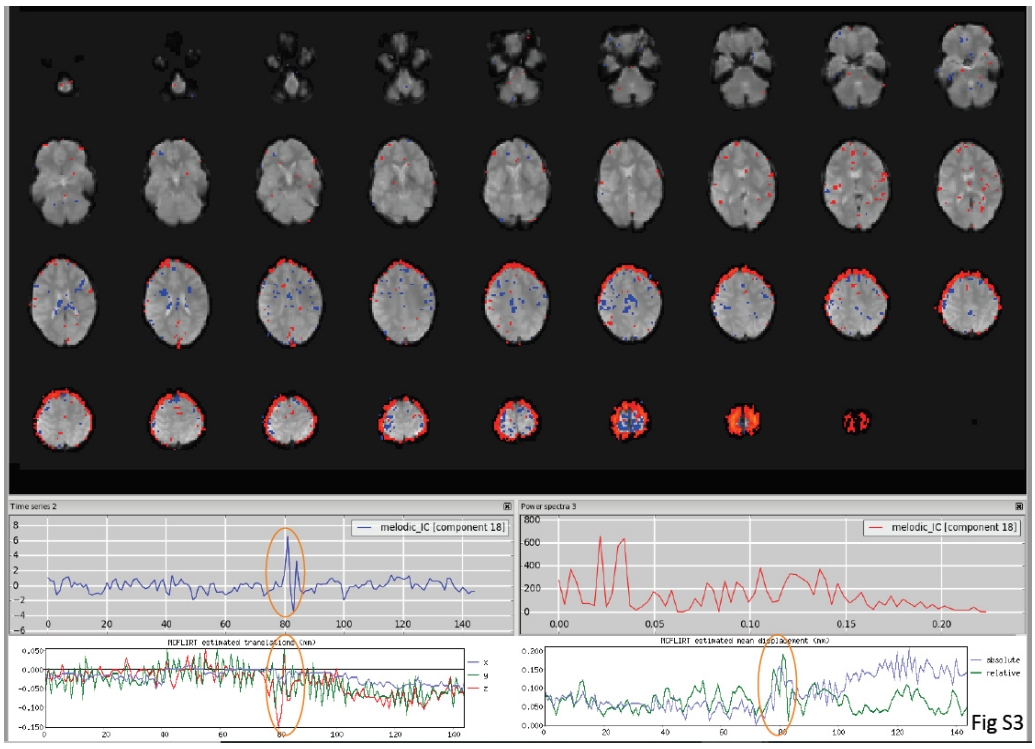

Figure 2.19. Motion artefact. The spatial map (top panel) presents the typical ring at the edge of the brain and the time series (bottom-left panel) contains a sudden jump in correspondence to sudden head movement (Griffanti et al., 2017).

❖ Cerebrospinal Fluid pulsation (Figure 2.20): the artefact is better identifiable in the spatial maps on the sagittal plane, where voxel activation can overlap the 4th ventricle and the cortical CSF at the pons level. The time series should show a high oscillation (indicative of the CSF pulsatile flow) and the power spectrum plot should be bell curved. This artefact is mainly caused by the respiratory cycle (around 0.3 Hz) and the cardiac cycle (around 1Hz), and the corresponding signals are typically aliased into lower frequencies.

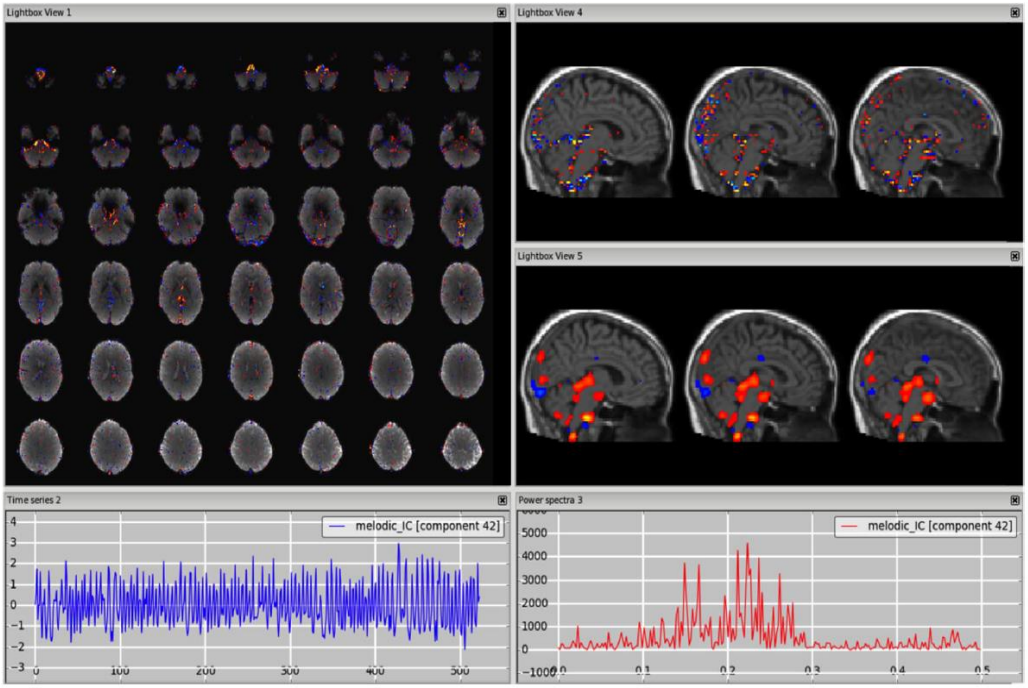

Figure 2.20. Cerebrospinal fluid pulsation. The spatial pattern overlaps the third and fourth ventricle. This is seen onto the structural image looking at different plane (top-left panel) and in the three ortho views before and after smoothing (respectively top-right and bottom-right panel). The time series shows a high oscillation pattern (bottom-left panel) and the frequency in the power spectra show a bell shape (bottom-right panel; Griffanti et al., 2017).

❖ Veins (Figure 2.21): The signal coming from the veins shows components with a saw-tooth pattern for the time series plot and a very low-frequency in the power spectrum plot, therefore similar to those of the neural signal components. For this reason, this artefact is mainly identifiable in the spatial maps on the sagittal plane, detected as physiological noise especially in the sagittal sinus and where are commonly identified the veins.

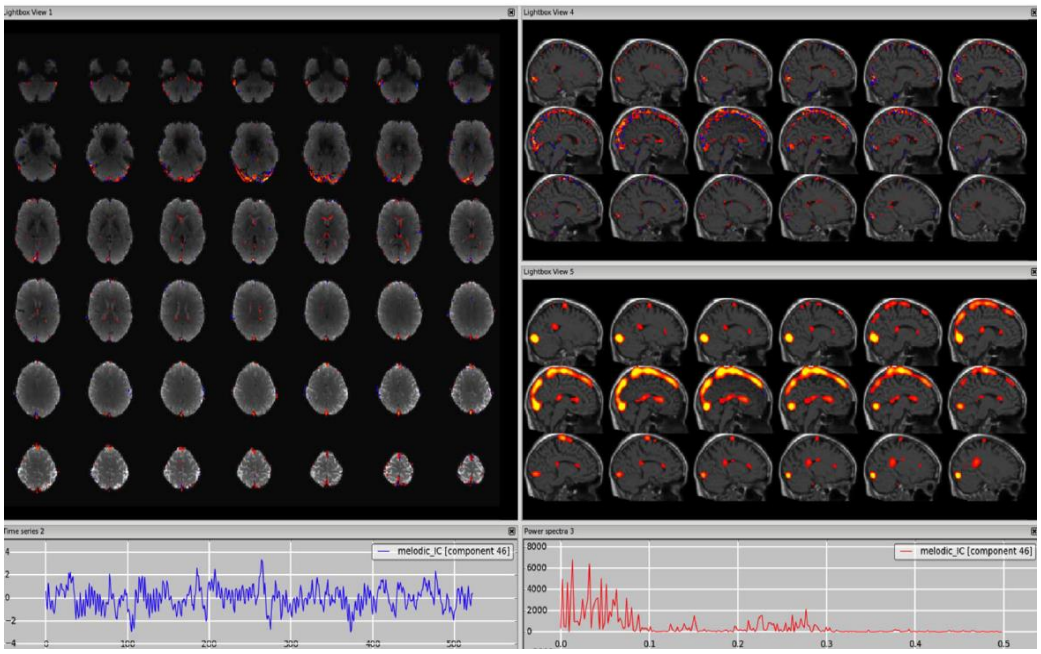

Figure 2.21. Vein (e.g., sagittal sinus). The vessel is most visible in the sagittal plane, as shown in top-right panel (before smoothing) and bottom-left panel (after smoothing; Griffanti et al., 2017).

❖ Arteries (Figure 2.22): Arteries and veins are considered cardiac artefacts and can present similarities to neural signals of interest due to the same blood related origin. As the veins, is important the knowledge of the anatomy of the brain vessel to identify the physiological noise. This artefact is mainly detectable in the power spectrum plot for the peak a frequency higher than 0.1 Hz and for the high-frequency pattern in the time series plot. Also, in the spatial maps, the active areas run close to the arteries.

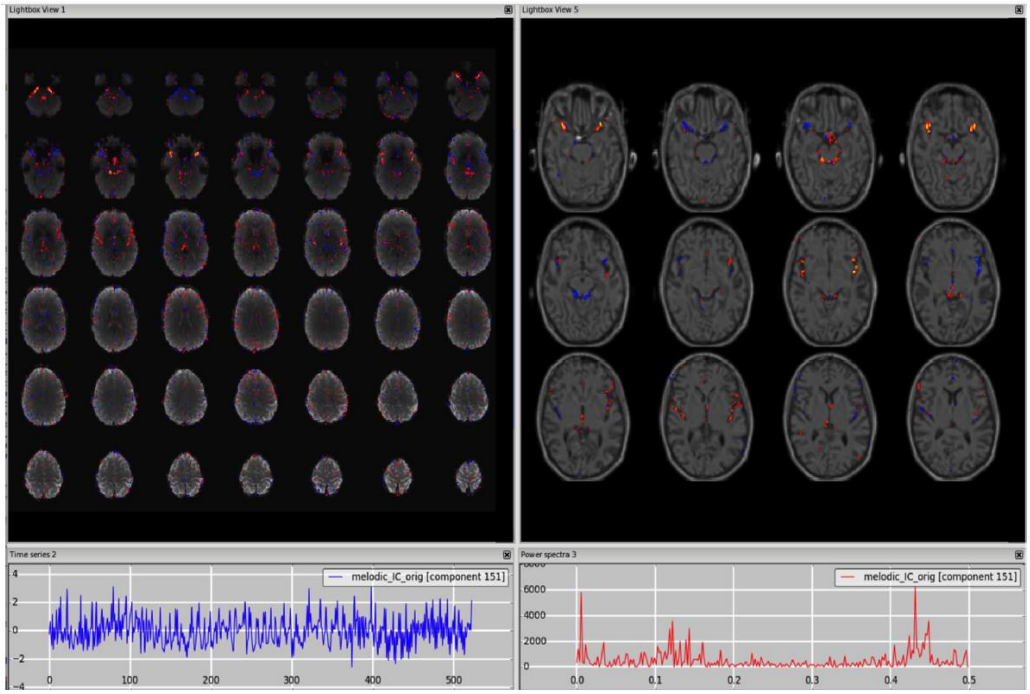

Figure 2.22. Arteries. The middle cerebral branches run close to the insula so a structural image as underlay can help localise the vessels (top panels). The time series shows a pattern with high oscillations (bottom-left panel) and the power spectra shows a high peak at high frequency, typical of the cardiac signal (Griffanti et al., 2017).

❖ Susceptibility artefacts (Figure 2.23): this kind of artefact is caused by signal drop due to the air-tissue interface, and for this reason better observed from the spatial maps on the axial (in the orbitofrontal gyrus and temporal poles, resulting from the eye and ear cavities respectively). There is one peak at a very low frequency, which is useful to detect the artefact.

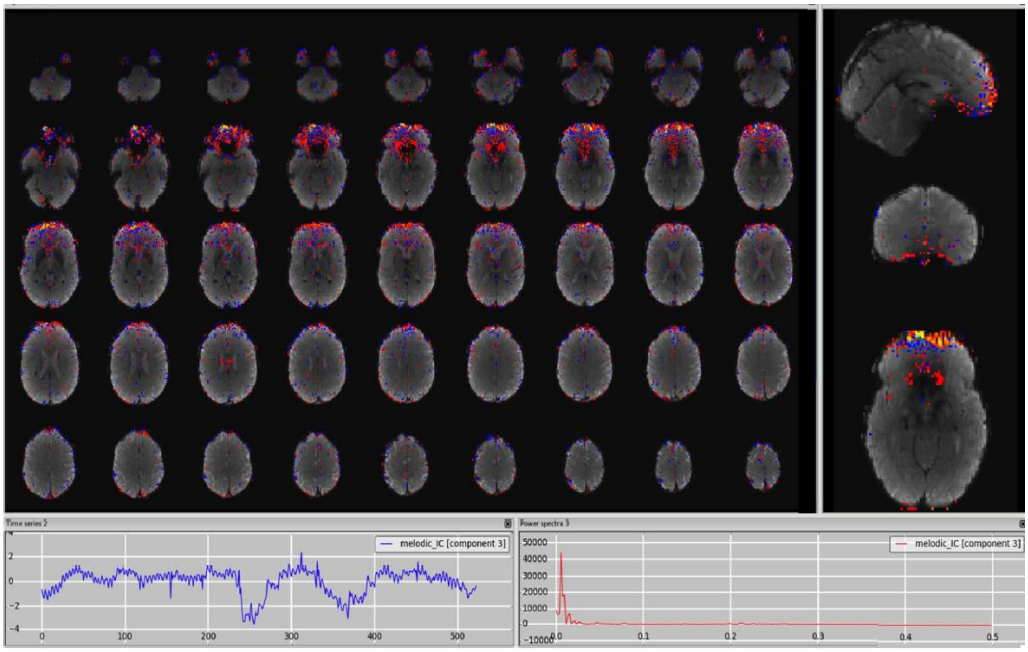

Figure 2.23. Susceptibility artefact. In the spatial maps this artefact is seen most clearly in the orbitofrontal gyrus where the signal drop (top panels). The power spectra show one peak at very low frequency (bottom-right panel; Griffanti et al., 2017).

❖ Multiband artefact (Figure 2.24): the simultaneous acquisition of multiple slices is the main cause of this artefact, which shows parallel lines of activity detectable in the spatial maps, mainly on the sagittal or coronal plane. This artefact can also depend on the characteristic of head motion, so the time course can show a sudden jump in correspondence of head movement, as for the motion artefact.

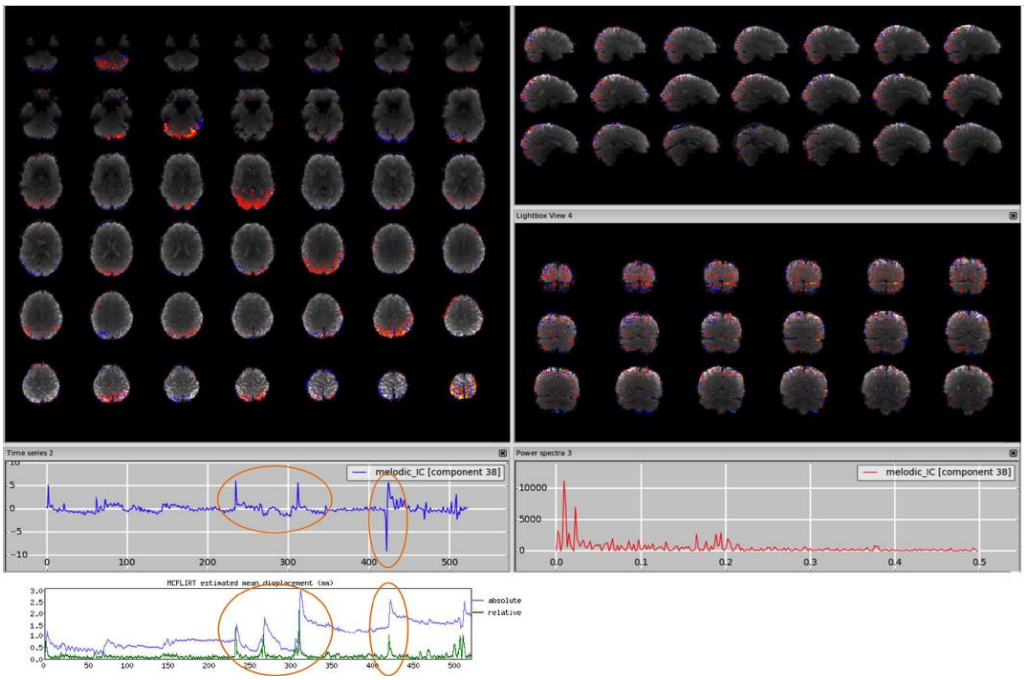

Figure 2.24. Multiband artefact. In the spatial maps the clusters are visible in a regular way across slices (top-left panel) and is reflected in stripes in the sagittal and coronal plane (top-right panel). The time series shows several sudden peaks in correspondence to head movement (bottom-left panel) and low-frequency peak in the power spectra (bottom-right panel; Griffanti et al., 2017).

❖ MRI-related artefact (Figure 2.25): This type of artefact is due to the MRI hardware or acquisition, and it does not shows any physiological activity in the spatial pattern, nor high frequencies in the time series plot; power spectrum plot is a bell curved at frequency greater than 0.1 Hz.

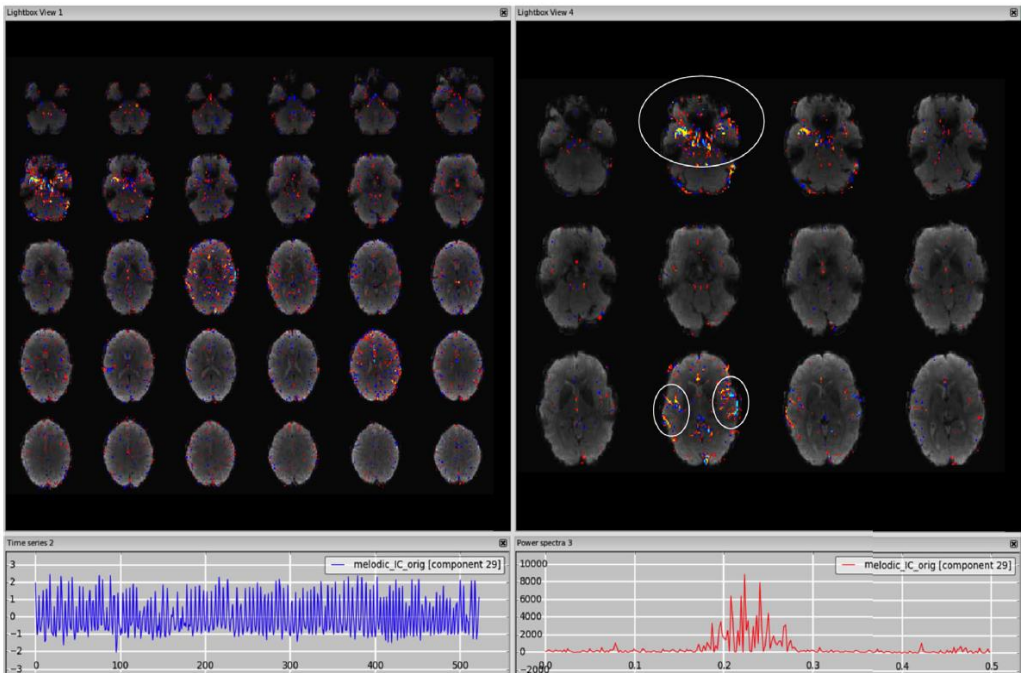

Figure 2.25. MRI-related artefact. The spatial map alternates between positive and negative values, as highlighted in the circles (top panels). The time series (bottom-left panel) and power spectra (bottom-right panel) have no physiological meaningful (Griffanti et al., 2017).

❖ Unclassified noise (Figure 2.26): If the components do not fit into any of the previous kind of signal (both neural and artefact), they are identified as unclassified noise.

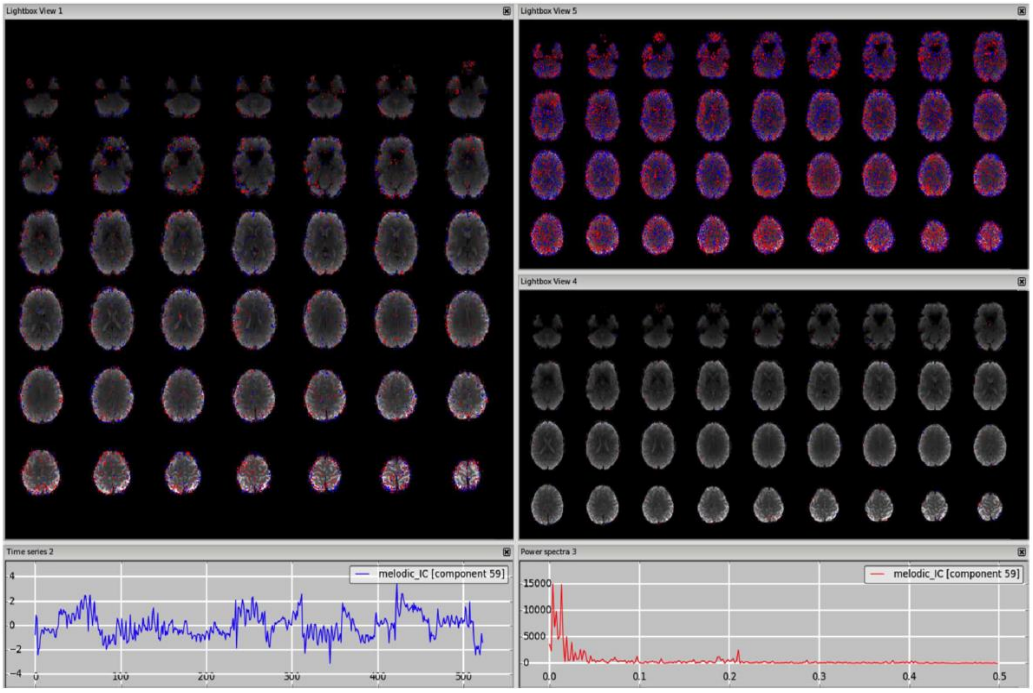

Figure 2.26. Unclassified noise. In this example the spatial map shows scattered cluster, typical of noise. The time series (bottom-left panel) show non-uniform pattern, with several temporal discontinuities and the power spectra has a low-frequency pattern (Griffanti et al., 2017).

❖ Unknown (Figure 2.27): If a component cannot be clearly classified as artefact (N-IC) or as signal (S-IC), for example a component containing both the neural signal and the noise or a component not perfectly coinciding with the most common networks presented but shows the features of neural signal, it is classified as unknown. The suggestion is to keep these kinds of components as signals of interest in the cleaning phase to avoid losing of valid signals, especially if the signal of the component is in the area essential for the study, and/or in case of altered neural activity (such as in the case of epileptic patients).

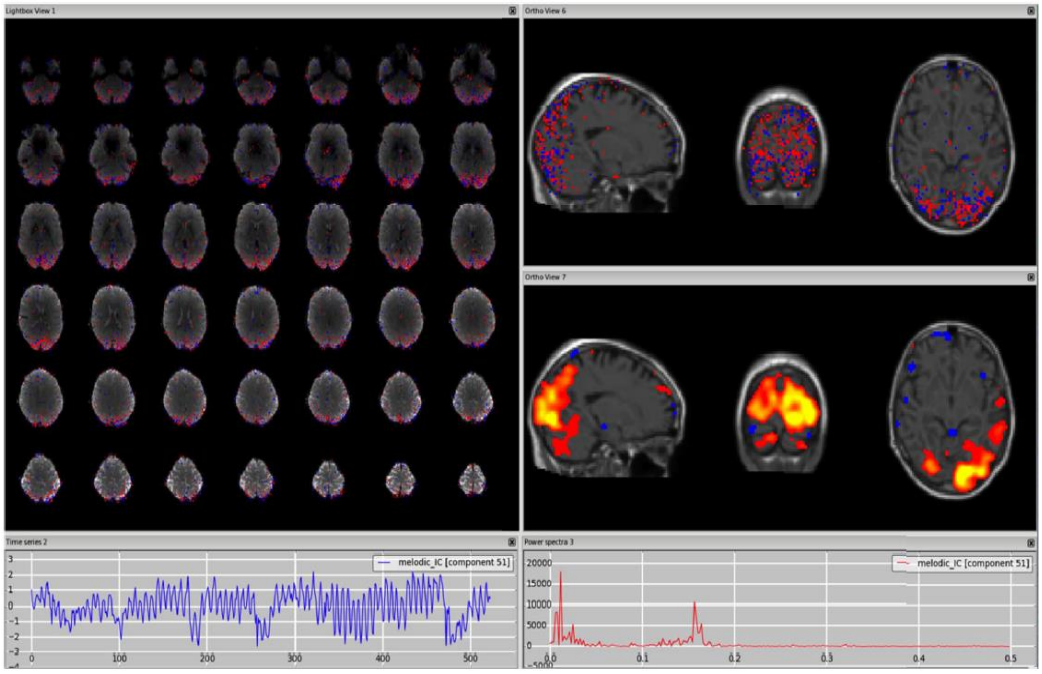

Figure 2.27. The spatial pattern is mainly localised in the grey matter, but is not clearly attributable to an RNS, both before (top-right panel) and after smoothing (bottom-right panel). The time series show a saw-tooth pattern with high oscillation (bottom-left panel) and the power spectra show both low and high frequency peak (Griffanti et al., 2017).

To distinguish the S-ICs from the N-ICs, it could be helpful to follow the "Innocent until proven guilty" flowchart in Figure 2.28 (Griffanti et al., 2017), which consists of a procedure to label components based upon visual inspection.

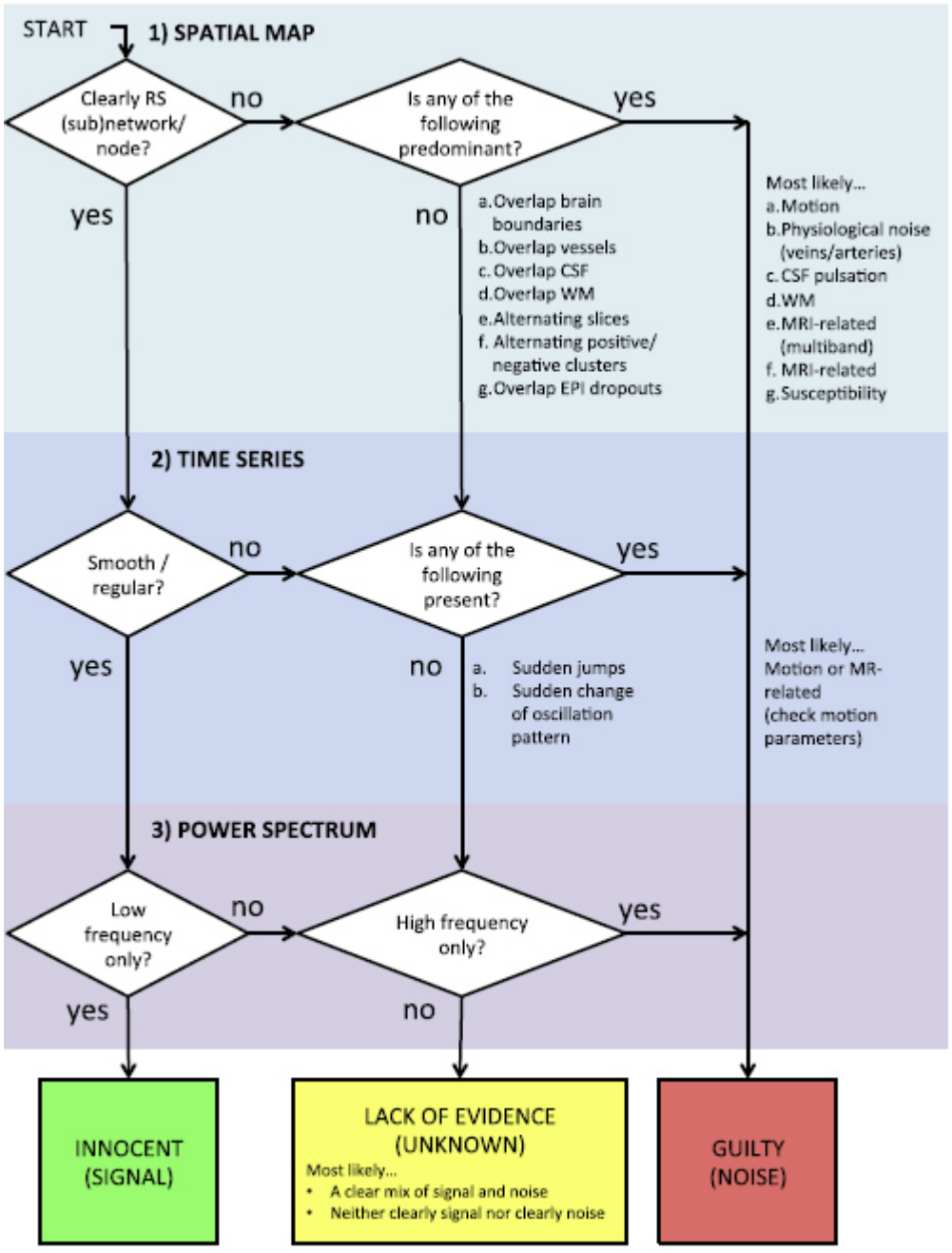

Figure 2.28. "Innocent until proven guilty" flowchart. A summary of the procedure for visual inspection and manual classification of independent components (Griffanti et al., 2017).

ICA-based cleaning is especially useful in resting state fMRI data, where there is no-priori information about the signal of interest (Griffanti et al., 2017).

3. Results

In this chapter the results obtained from the analysis described in the chapter 2 are reported. Firstly, the motion correction and registration are examined and if they satisfy the requirements, it is possible to proceed with the inspection of IC. After the recognition of artefact, the RSNs were detected by a comparison with the RSNs identified by Smith and coworkers (Smith et al., 2009) and Beckmann and coworkers (Beckmann et al., 2005).

3.1 Pre-processing results

The subject P6 was excluded from the study because there was an error in the functional data acquisition.

The subject P5 was excluded from the study because there is a significant displacement around the volume 230, principally around the x-axis and along the x and y axes, as shown in Figure 3.1, obtained from MCFLIRT within FSL.

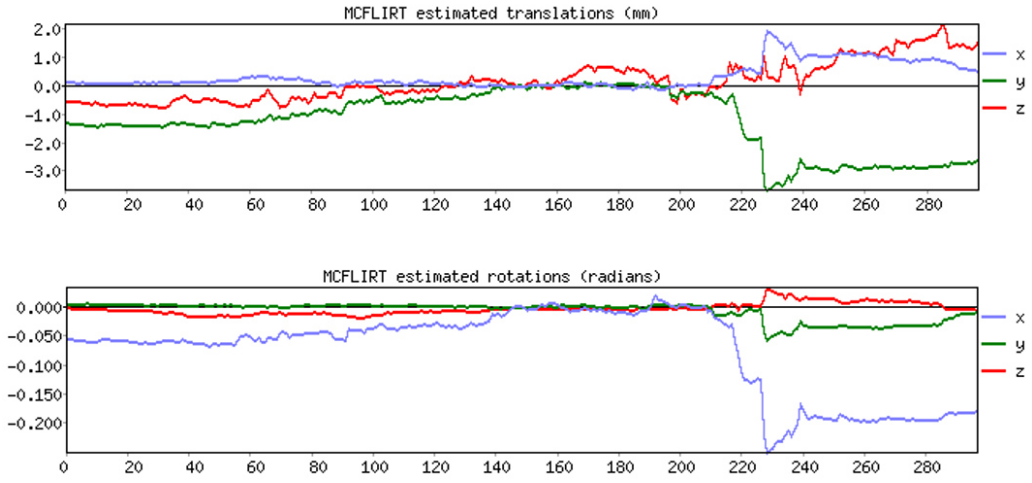

Figure 3.1. The displacement detected in the subject P5. The upper panel indicates the translation movement along the axes. The lower panel indicates the rotation movement around the axes.

All the other patients (P1, P2, P3 and P4) hace an acceptable head movement and are suitable to continue the analysis.

In Figure 3.2 the displacement of P1 is reported: a peak of movement around the volumes 290 can be noted, an initial displacement in rotation around x and y axes, but it is an acceptable movement. All the peak results in the IC as motion artefact.

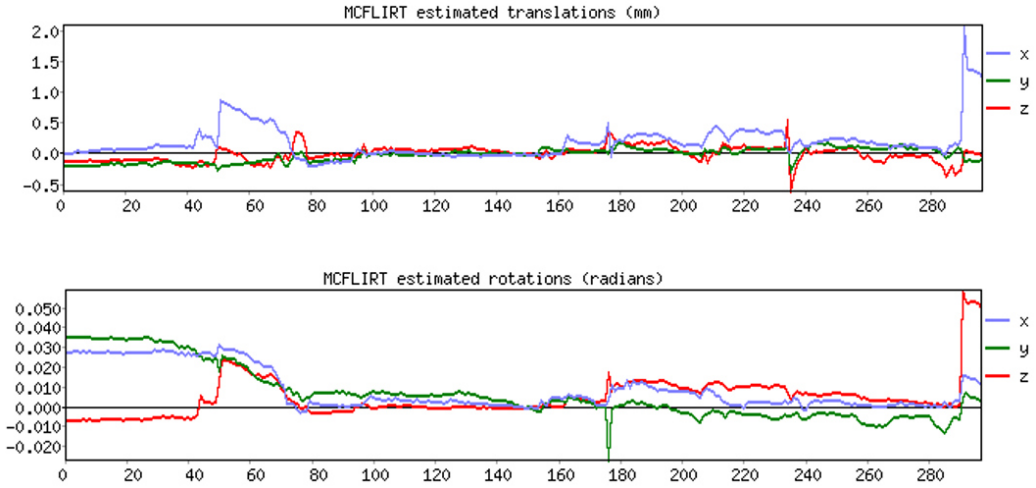

Figure 3.2. The displacement detected in the subject P1, suitable for further analysis. The top panel indicates the movement along the axes. The bottom panel indicates the movement around the axes.

Figure 3.3 shows the movement of P2, showing an initial displacement which tends to zero.

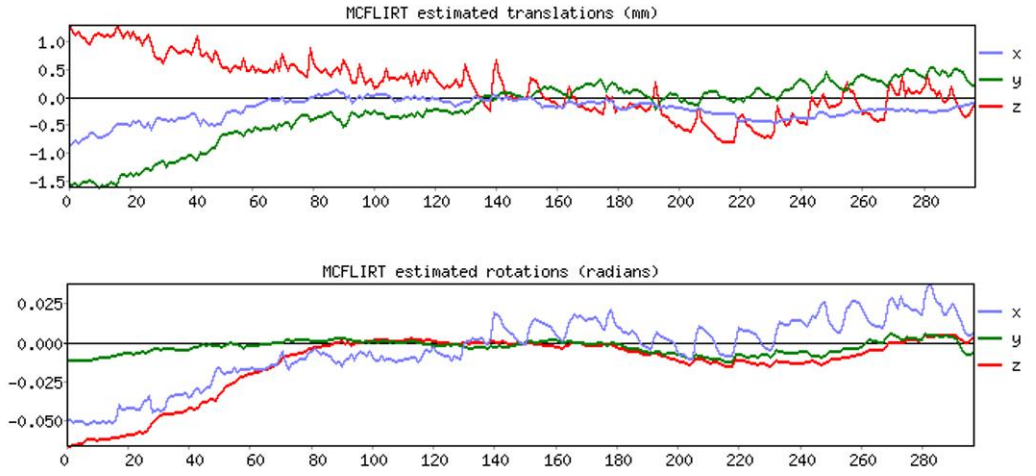

Figure 3.3. The displacement detected in the subject P2. The above panel indicates the rotation movement around the axes. The panel below indicates the translation movement along the axes.

The head movement of P3 is shown in Figure 3.4. The displacement is low, in a range around zero, as for patient P4, shown in Figure 3.5.

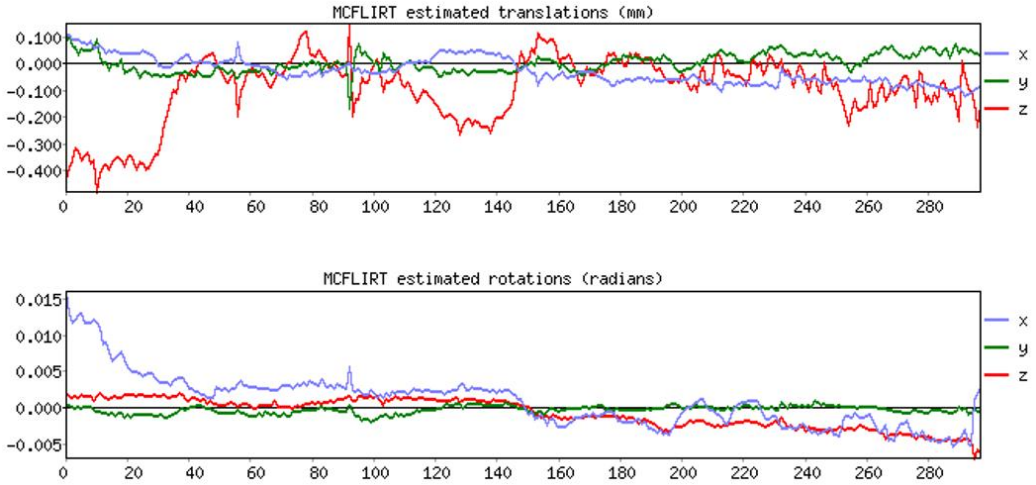

Figure 3.4. The displacement detected in the subject P3. The above panel indicates the rotation movement around the axes. The panel below indicates the translation movement along the axes.

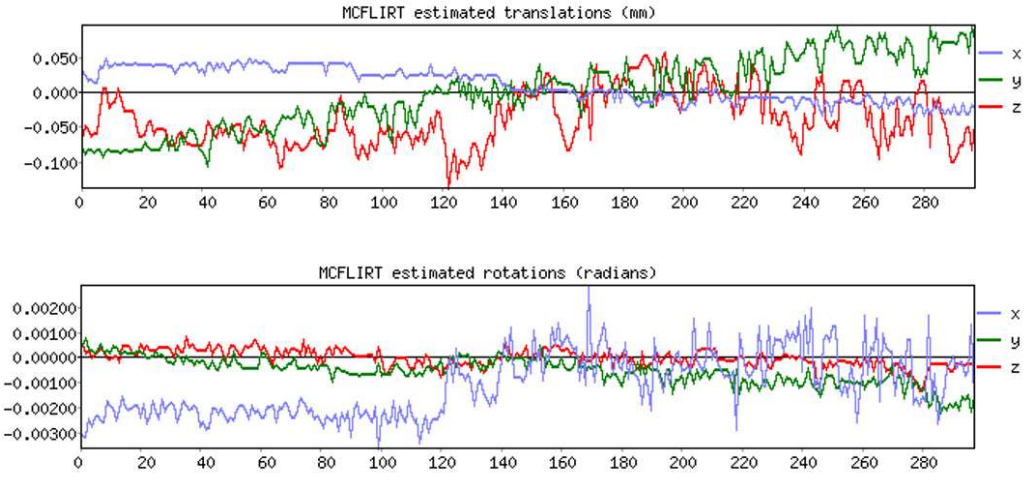

Figure 3.5. The displacement detected in the subject P4. The above panel indicates the rotation movement around the axes. The panel below indicates the translation movement along the axes.

The registration step was successful for all the subjects. An example of registration within FSL is shown in Figure 3.6, and within BV in Figure 3.7.

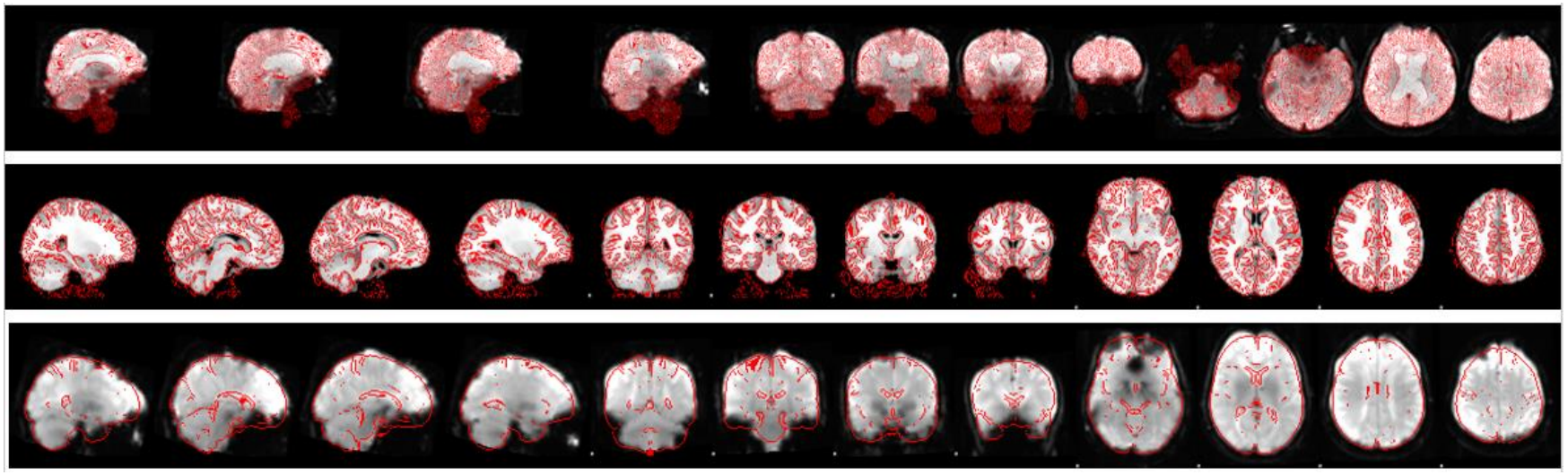

Figure 3.6. The top panel represents the coregistration of functional image (in grey) in structural BET image (red line). The middle panel represents the MNI152 template (in grey) in structural BET image (red line). The bottom panel represents the normalization of functional image (in grey) in the MNI152 template (red line).

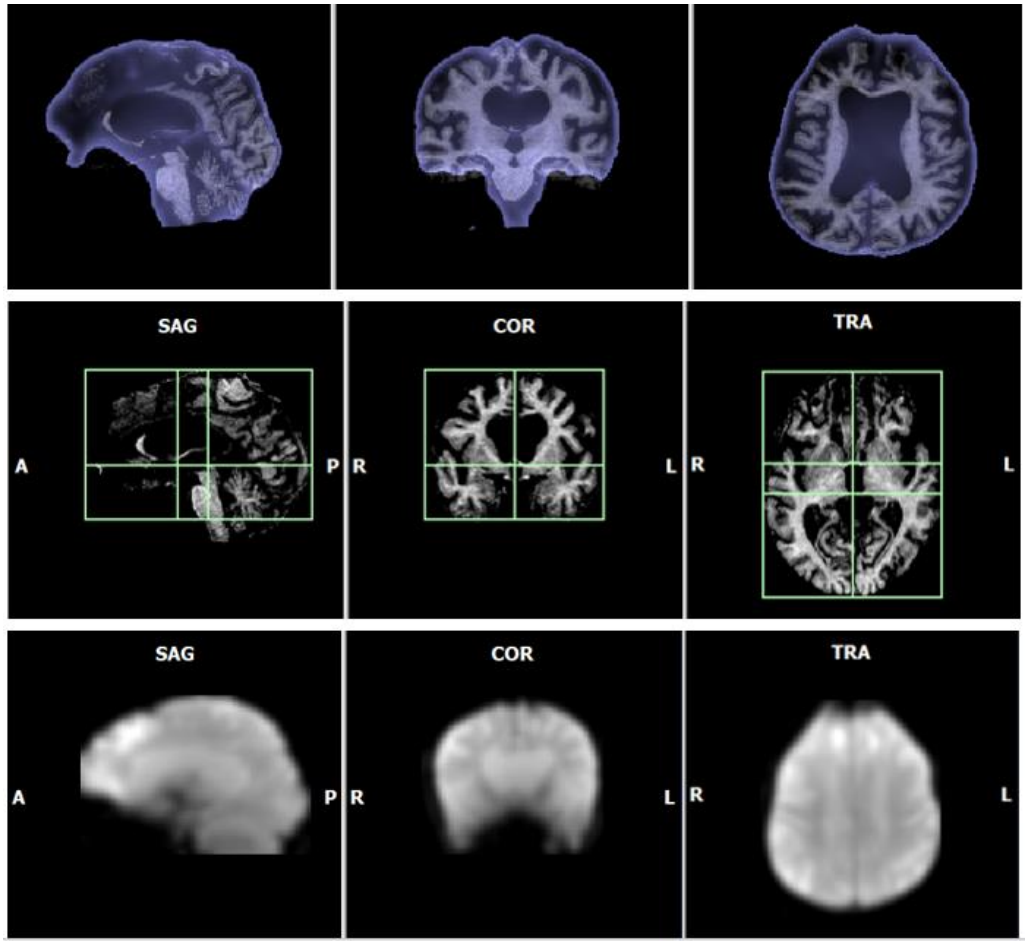

Figure 3.7. The top panel represents the coregistration of functional pre-processed file (trasparent) in structural IIHC image. The middle panel represents the structural IIHC image in Talairach space (green lines). The bottom panel represents the normalization of functional image (in grey) in the Talairach space.

3.2 Independent Components Analysis

3.2.1 FSL

The number of estimated ICs within FSL software was different for each subject: specifically, 71 ICs were obtained from the analysis on subject P1, 95 ICs were obtained from ICA on subject P2, 70 ICs estimated on subject P3, and 41 ICs from subject P4. A total of 277 components were identified: 204 (74%) were labelled N-IC, 73 (27%) were labelled S-IC (30 ICs were signal of interest (11%), 43 unknown (16%)).

Each component was meticulously examined within FSLeyes, which is an image viewer tool of FSL (McCarthy, 2021), in the Melodic view and in the Ortho

view. By applying the labelling rules states by Griffanti and coworkers (Griffanti et al., 2017; Figure 2.28), each slice, time courses and frequency spectra were examined and labelled as Signal, Unknown and Noise. An example of N-IC is shown in Figure 3.8 and an example of S-IC in Figure 3.9. Both figures show the Time series (bottom-left panel), the Power spectra (bottom-right panel), the axial slices in top-left panel (can be moved to coronal and sagittal plane), and the ortho view (top-right panel). The red/yellow activation are overlayed onto the MNI152 template.

The Z-score is greater than 2 and lower than 10. To investigate similarities in S-ICs between each subject and RSNs by Smith and coworkers (Smith et al., 2009) the command line "fslcc" was used. This fslutils run a cross-correlations between every volume in the subject's data with every volume in the Smith's Networks. The S-ICs obtained corresponding to well-established RSNs are represented in Figure 3.10, Figure 3.11, and Figure 3.12. In each figure, RSNs is indicated on the top; different rows refer to different patients. The images are shown in radiological convention and the MNI coordinated indicated in the image caption. Medial, Occipital and Lateral Visual Area show a low degree of bilaterality, with a predominance of activity in the right hemisphere. DMN is mostly lateralized, except for a slight bilateral activity in P1. P2 and P3 show activity only in the left hemisphere, whereas P4 only in the right. Sensorimotor system was detected only in two subjects, with a lateralized active area in the right hemisphere for P1 and a low bilateral activity in P2. Auditory system was identified in three subjects, mostly with bilateral activity (P1 and P3), but strongly lateralized in P2. Executive control network shows high degree of bilaterality, but it was identified only in P1. Frontoparietal right and left network are exclusive lateralized in right and left hemisphere, respectively. Table 3 summarize the RSNs identified among all the S-ICs of each subject.

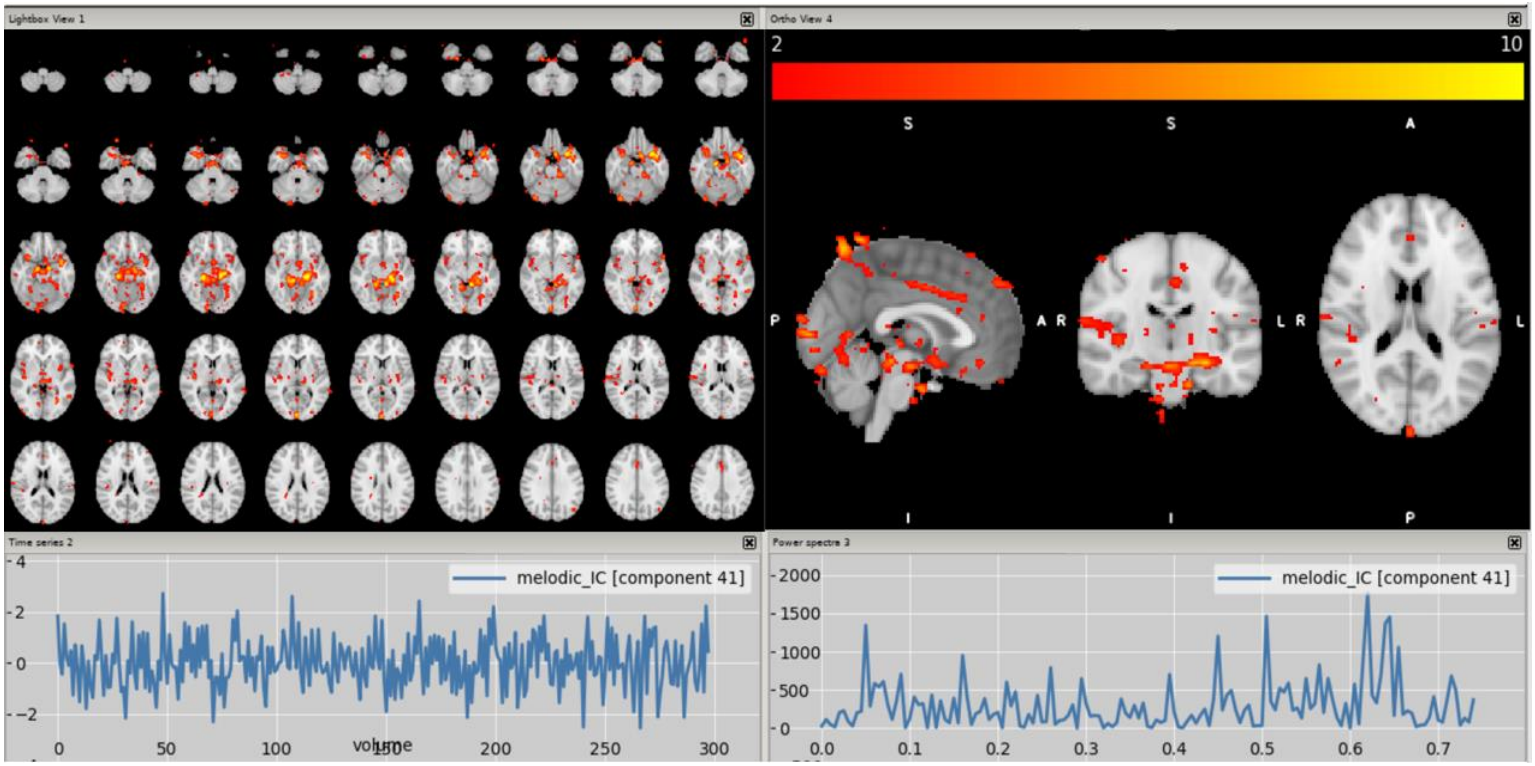

Figure 3.8. An example of noise component analysed by using FSLeyes. This component is considered artefact because the frequency is higher than 0.1 Hz and the activated area are localized mostly around the brain.

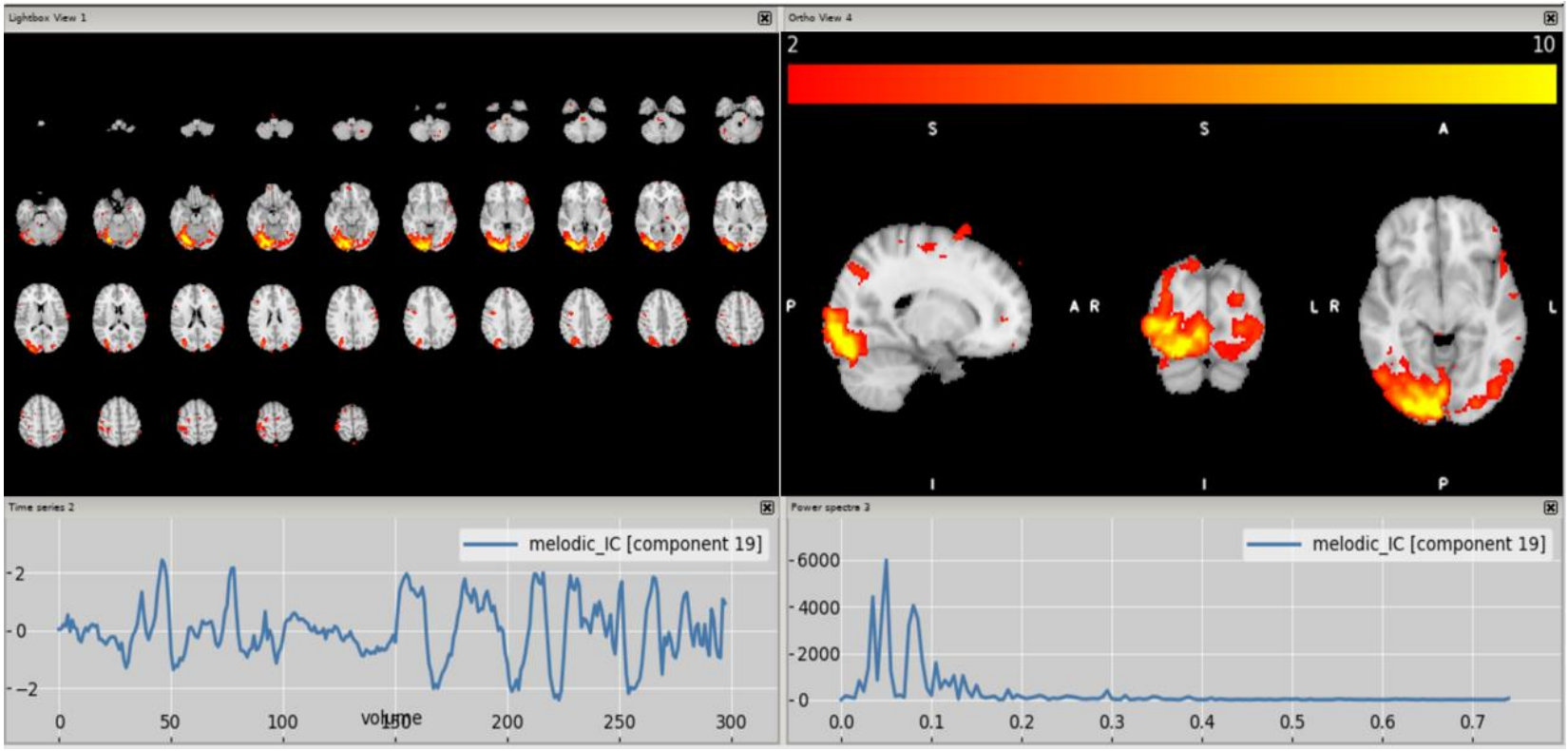

Figure 3.9. An example of signal component. The components are characterized by a regular oscillatory time, frequency lower than 0.1 Hz, and the spatial maps show an activated area across slices and on grey matter.

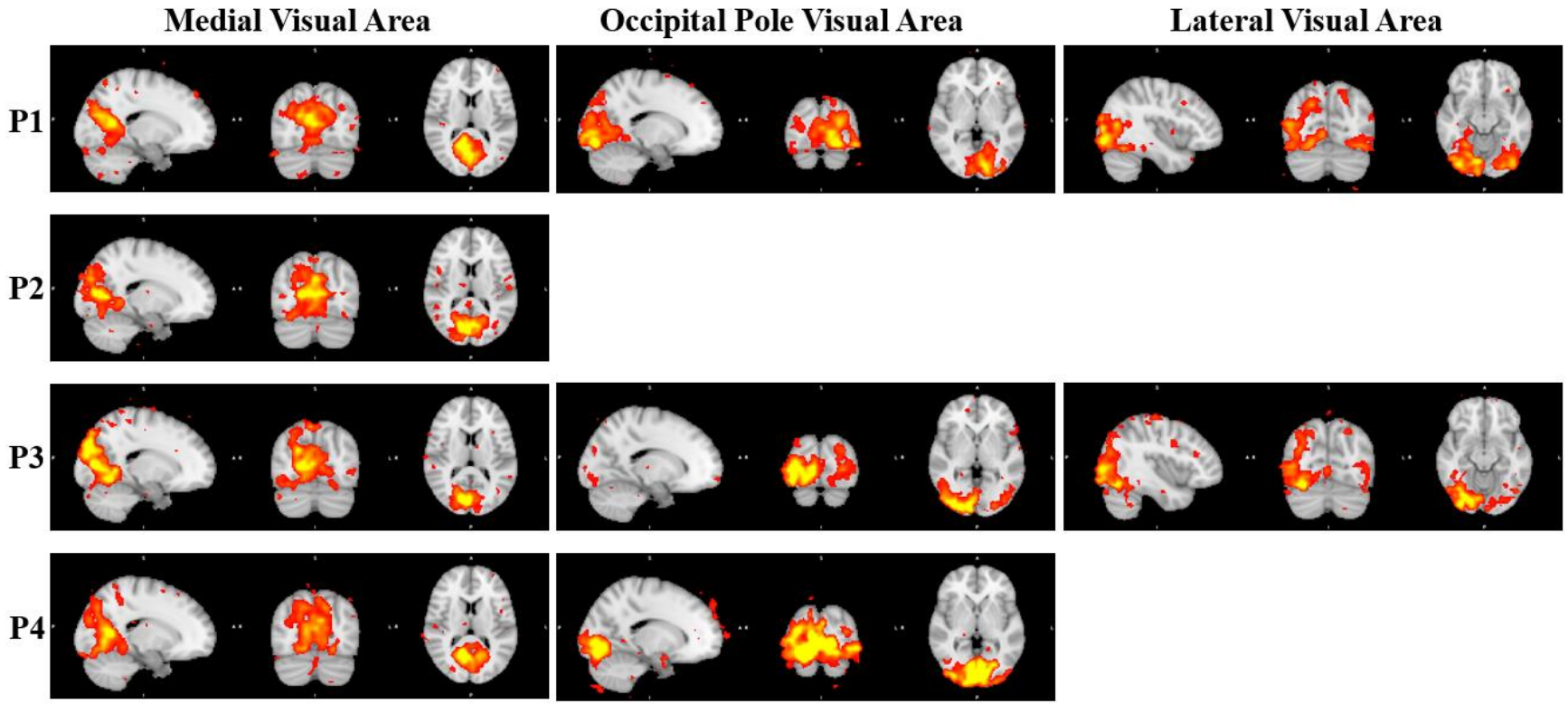

Figure 3.10. The MNI coordinates are: Medial Visual Area (17, -73, 10), Occipital Pole Visual Area (-17, -88, 0), Lateral Visual Area (39, -71, -12).

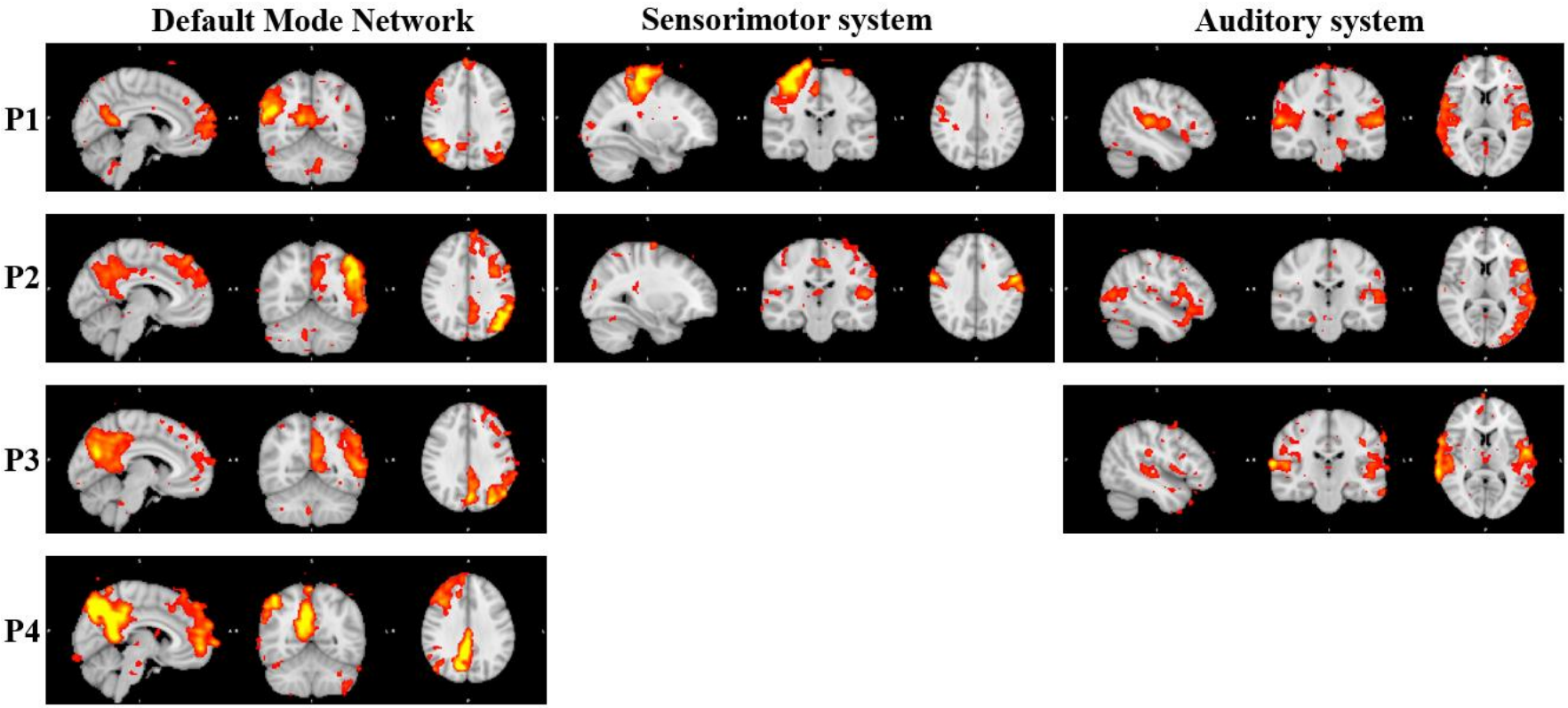

Figure 3.11. The MNI coordinates are: Default Mode Network (-6, -55, 33 to P2 and P3, and -6, -55, 33 for P1 and P4), Sensorimotor System (30, -22, 34), Auditory System (-47, -22, 8).

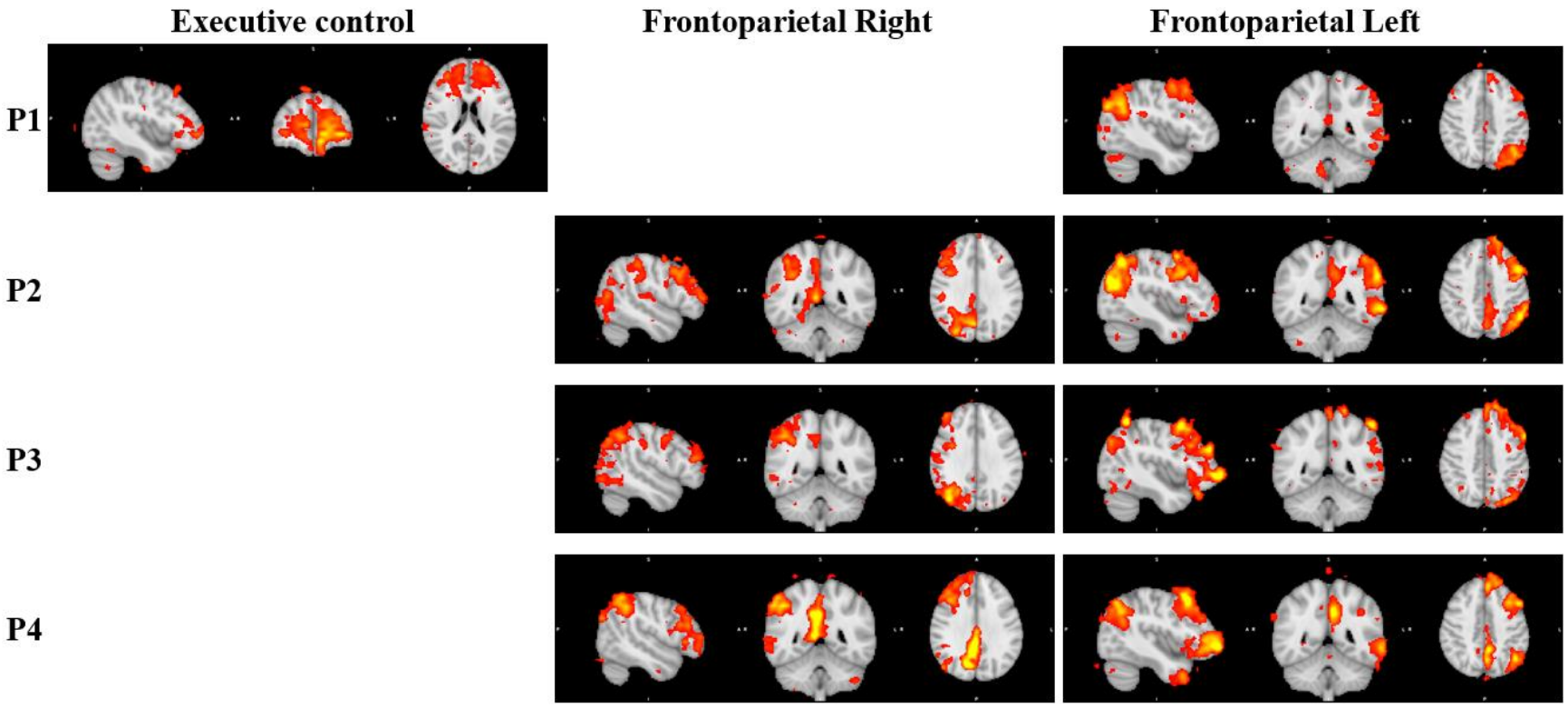

Figure 3.12. The MNI coordinates are: Executive control (-43, 50, 20), Frontoparietal Right (49, -48, 32), Frontoparietal Left (-43, -48, 42).

It can be noted that the Medial Visual Area, the DMN, and the Frontoparietal Left were identified in all patients, whereas the Executive Control in only one subject.

Table 3. RSNs identified in all subjects by using FSL analysis.

	P1	P2	P3	P4
Medial Visual Area	✔	✔	✔	✔
Occipital Pole Visual Area	✔		✔	✔
Lateral Visual Area	✔		✔	
Default Mode Network	✔	✔	✔	✔
Sensorimotor system	✔	✔		
Auditory System	✔	✔	✔	
Executive Control	✔			
Frontoparietal Right		✔	✔	✔
Frontoparietal Left	✔	✔	✔	✔

3.2.2 BrainVoyager

The number of ICs estimated within BV software was 30 for all subjects, for a total of 120 components: 103 (86%) were labelled as artefact and 17 as S-IC (10 ICs were signal of interest (8%), and 7 unknown (6%).

The spatial map in the ortho view and the time series of each component were examined and, by applying the labelling rules states by Griffanti and coworkers (Griffanti et al., 2017; Figure 2.28), classified as Signal and Noise. An example of N-IC is shown in Figure 3.13 and an example of S-IC in Figure 3.14. In both figures the Time series (bottom panel) and the ortho view (top panel) are shown. The red/yellow activation are overimposed onto the structural image of the subjects, transformed in Talairach space. The Z-score index was greater than 2 and lower than 10 (same scale used within FSL).

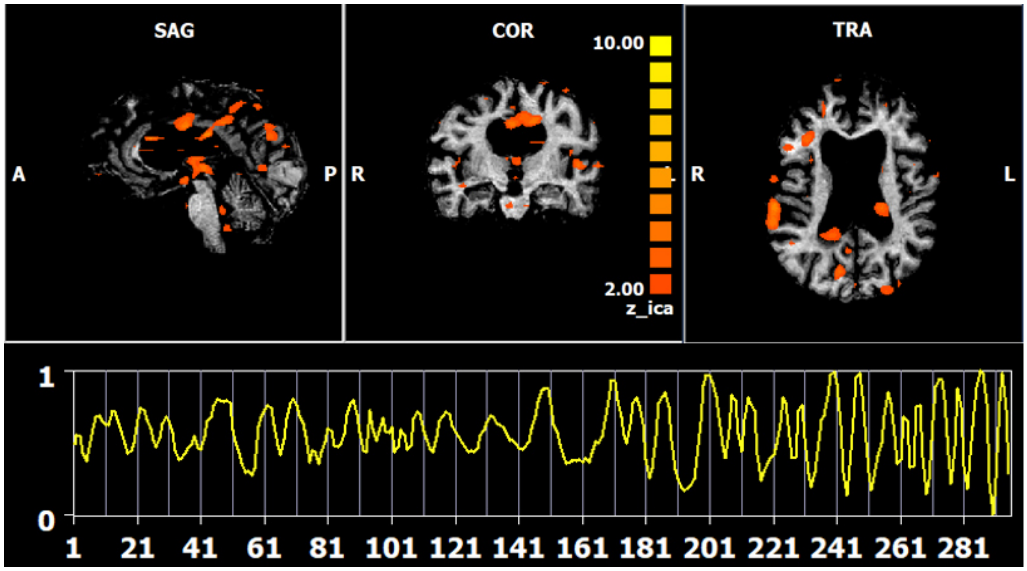

Figure 3.13. An example of artefact component. In the spatial map the clusters are localised in the white matter (top panel). The time series shows a high oscillation, especially in the last volume.

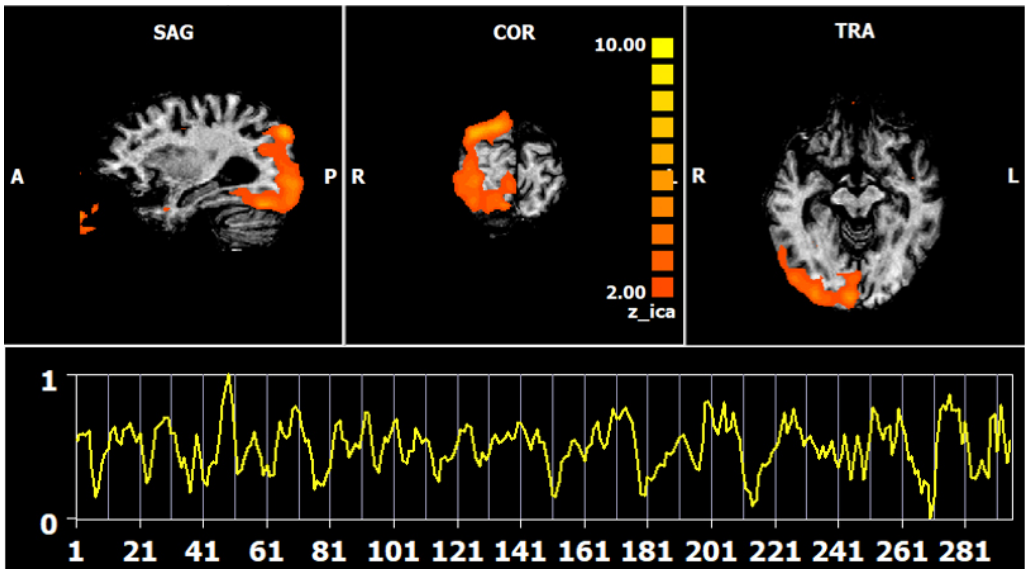

Figure 3.14. An example of signal component. The clusters in the spatial map are in the grey matter (top panel). The time series shows a typical saw-tooth pattern (bottom panel).

The S-ICs obtained that correspond to well-established RSNs, according to Smith (Smith et al., 2009), are manually detected and are represented in Figures 3.15, 3.16, 3.17, and 3.18. Each network is shown in the sagittal, coronal, and axial view and the Talairach coordinates are reported in the image caption. The images are shown in radiological convention.

The networks identified in P1 were three: the Executive control network, which shows low bilaterality with a greater activity in the left hemisphere; the Auditory system, with a low degree of bilaterality mainly active in the left hemisphere; the Sensorimotor system, which shows bilateral activity.

Three networks were recognized in P2: Visual network (mostly lateral and occipital lobe), showing strongly lateralized activity in the left hemisphere; the Frontoparietal Right and Left, which showing activity only in the right and left hemisphere, respectively.

From the analysis performed on subject P3 three networks were identified: Lateral visual area, showing activity only in the right hemisphere; Auditory system, showing bilateral activity, but mainly in the right hemisphere; the Frontoparietal right, showing active areas only in the right hemisphere.

Finally, only two networks were detected in the subject P4: Occipital Pole visual area, with high degree of bilaterality, and the DMN, localized only in the right hemisphere. Table 3 summarize the RSNs identified among all the subjects.

Table 3. RSNs identified in all subjects by using BrainVoyager software.

	P1	P2	P3	P4
Medial Visual Area				
Occipital Pole Visual Area		✔		✔
Lateral Visual Area		✔	✔	
Default Mode Network				✔
Sensorimotor system	✔			
Auditory System	✔		✔	
Executive Control	✔			
Frontoparietal Right		✔	✔	
Frontoparietal Left		✔		

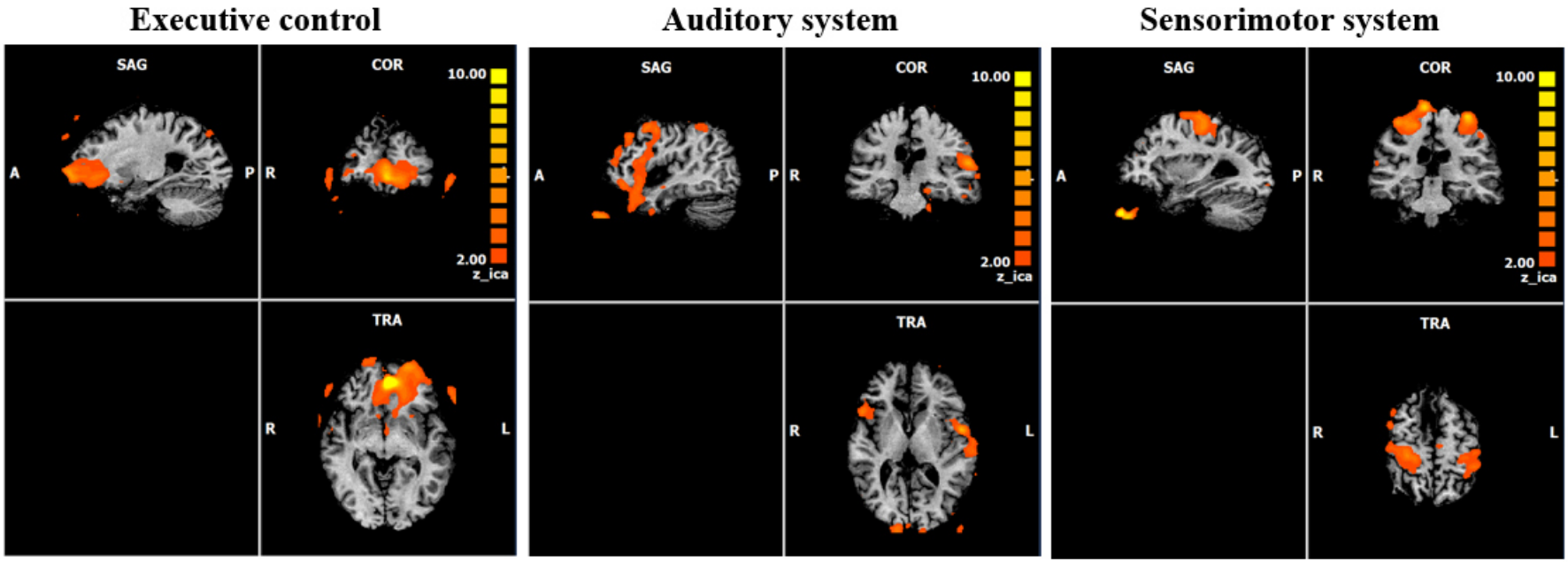

Figure 3.15. RSNs identified in P1 subject. The Talairach coordinates are: Executive Control (-18, 40, -4), Auditory system (40, -23, 6), Sensorimotor system (29, -26, 48).

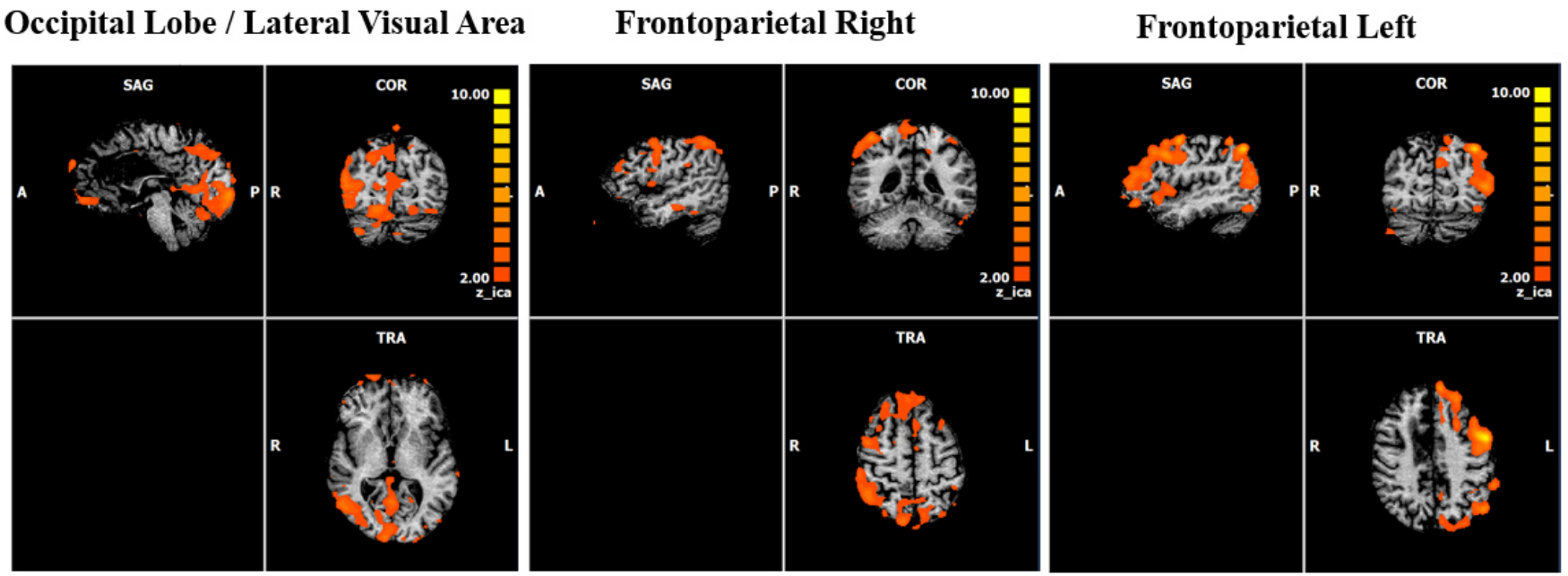

Figure 3.16. RSNs identified in P2 subject. The Talairach coordinates are: Occipital Lobe / Lateral Visual Area (3, -67, 3), Frontoparietal Right (46, -43, 49), Frontoparietal Left (-43, -67, 36).

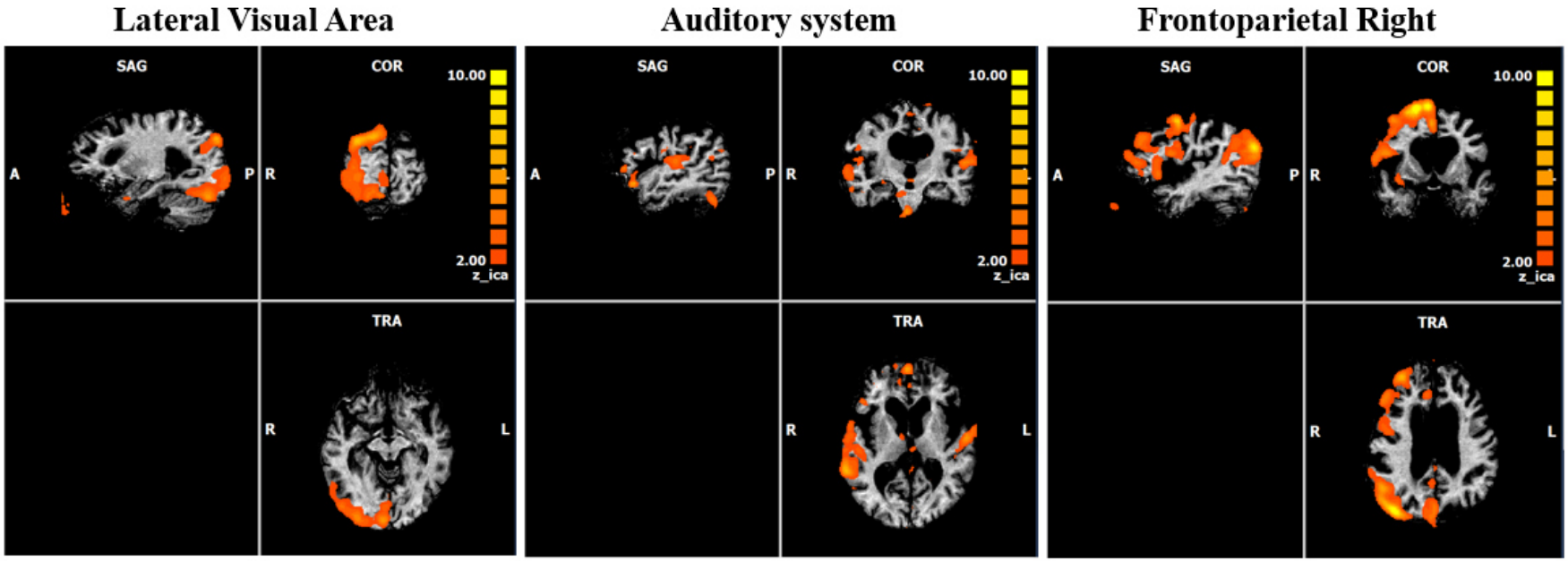

Figure 3.17. RSNs identified in P3 subject. The Talairach coordinates are: Lateral Visual Area (24, -83, -7), Auditory system (48, -14, 8), Frontoparietal Right (27, 14, 28).

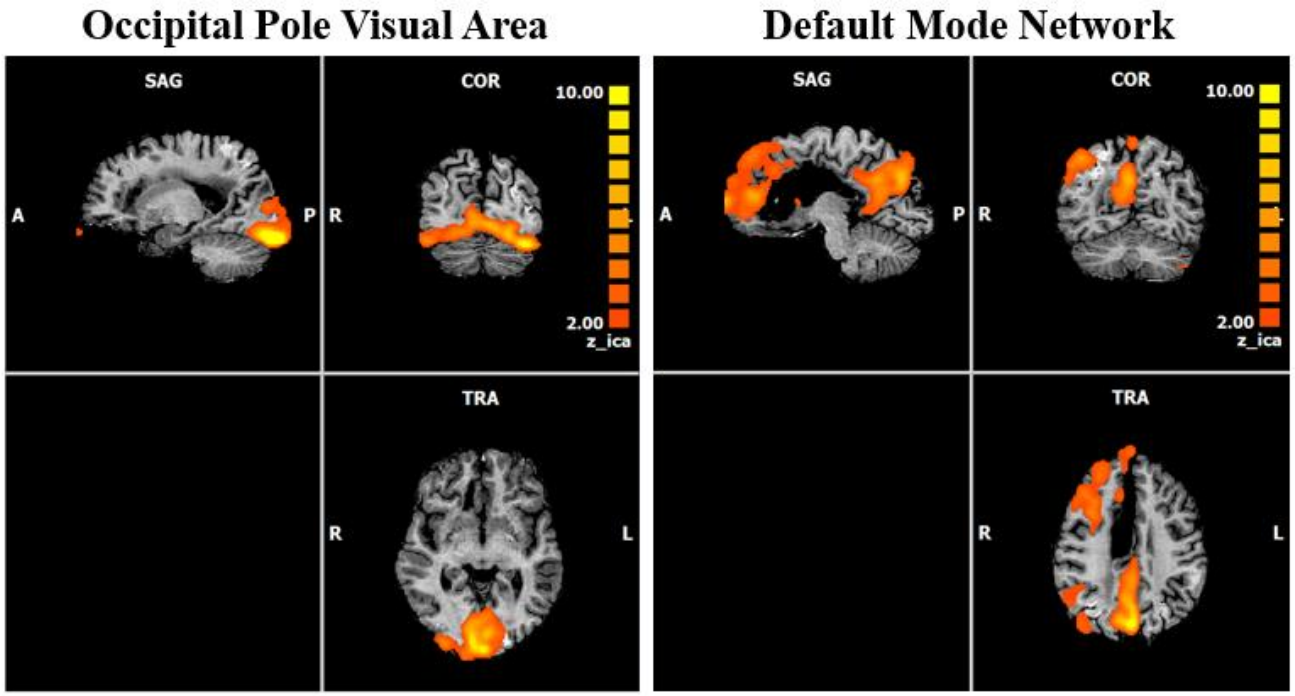

Figure 3.18. RSNs identified in P4 subject. The Talairach coordinates are: Occipital Pole Visual Area (-17, -71, -4), Default Mode Network (7, -56, 30).

4. Discussions

The aim of this Thesis is to investigate the interhemispheric functional connectivity in a set of split-brain subjects, based on the analysis of resting-state fMRI data by using the ICA approach.

One of the most evident characteristics of FC in resting state is the symmetry about the midline. Since the CC is the major brain commissure connecting the two hemispheres, it is logic to assume that it plays the central role in the symmetric features of FC.

The analysis was performed on 4 subjects who had undergone to callosotomy about two decades before. The results showed in most cases a low degree of bilaterality in the RSNs. A partially preserved interhemispheric connectivity was found in the visual areas and the auditory network. Across our subjects, more neural activity was noted in the right hemisphere than the left. Based on the theory of brain lateralization, the right hemisphere is more involved in the space cognition, spatial visualization and vision perception of object motion and shape around us. Some other networks are entirely lateralized across all subjects, as Frontoparietal right and left and the DMN. The Frontoparietal left networks was identified in all subjects. The left hemisphere is strongly specialized in language comprehension and speech production. The DMN was identified in all subjects, in left hemisphere in two, in right in one and bilateral in the last patient. The DMN in healthy subject is a strongly bilateral network; it is associated with cognitive processes, such as introspection, image the future or remember the past. It is active only during rest phase, when the person is relaxing. The DMN's integrity seems to be crucial for mental health. In the present set of patients, the neural brain activity of this network is less lateralized, likely because of the callosotomy or of the drug treatment for epilepsy; therefore, the FC of this network is slightly altered.

Technical considerations

Many studies have demonstrated that an ICA decomposition can be used to identify patterns of activation, including RSNs, and image artefacts (Beckmann and Smith, 2004; Beckmann et al., 2005; Robert et al., 2010). However, ICs are influenced by multiple factors related to the subjects (if has some disorder or not), the MRI data acquisition and the pre-processing.

The number of ICs automatic estimated within MELODIC is different across the subjects mainly due to the different degree of head motion. When the data are particularly corrupted by one or more artefact (as in the case of P2), the ICA algorithm creates many components that are not clearly identifiable, leading to an overfitting of components. A great number of ICs could lead to a RSNs to split into multiple sub-networks and therefore more difficult to identify.

At the same time, the number of ICs estimated within BV software are few, leading the case of underfitting, that means the number is insufficient to obtain a good estimation of signal. In fact, in BV 86% of ICs were labelled as artefact and only the 8% as signal of interest, whereas in FSL the percentage of components classified as artefact is lower, around the 74% and the components labelled as signal of interest around the 11%.

In this thesis an automatic classifier to label the IC was not used, but it was preferred the hand classification because the "non-conventional datasets". The advantage of this method is the possibility to investigate each component individually to detect the neural networks in a case of patients with altered brain activity. However, the visual inspection is time consuming and also quite subjective. Actually, some ICs can contain a mix of signal and noise and could be discarded, but they should be classified as "unknown" and kept in the analysis, especially if they are in the area of study (Griffanti et al., 2017).

Comparison with other studies.

In literature there are various studies conducted on human with callosal alteration, which can be either callosal agenesis (AgCC) or callosal resection. Callosal agenesis is a rare congenital disorder, characterised by a partial or

complete absence of CC. Most of studies carried out in CC agenesis patients emphasize that in these patients FC is similar to that of intact brain subjects. As shown in recent study (Owen et al., 2013), most networks have been identified to show bilateral activity, but some regions involved in the Frontoparietal right and left and DMN show reduced FC. Another study (Tyszka et al., 2011) demonstrated that the RSNs identified in the AgCC subjects correspond to networks identified in healthy subject.
Different results were obtained from studies carried out on subject whose CC was resected during their lifetime to treat intractable epilepsy: some studies reported the loss of interhemispheric FC, others found some bilateral activity.

Specifically, Uddin and colleagues (Uddin et al., 2008) found a strong bilateral connectivity in Visual Networks, and less but present bilateral connectivity in DMN, in one old patient studied four decades after total callosotomy. Another recent study (Hung et al., 2019), conducted on a group of paediatric patients 4 months after a total callosotomy surgery, found a partial bilateral connectivity especially in the frontal and anterior temporal lobes. Moreover, they state the interhemispheric FC could recovers in the first years after surgery (up to 16 years old), mainly if the anterior commissure is preserved.
The studies performed on AgCC patients indicate that the callosotomy does not have a drastic effect on the interhemispheric functional connectivity, mainly because in these patients the absence of CC is congenital, and the functional networks can develop progressively as the patients grow. These studies suggest that CC is not the only path involved in interhemispheric functional connectivity, and in its absence some other cortical subcortical pathway takes, care of transferring information between hemispheres. Therefore, the RSNs and normal cognition can emerge even under circumstances where the structural base is disrupted.
On the other hand, the literature results about the FC in the callosotomized subjects are conflicting. At variance with the above-mentioned researches (Uddin et al., 2008; Hung et al., 2019), other studies, (Johnston et al., 2008; Roland et al., 2017), both carried out in paediatric patients, found a loss of resting

interhemispheric FC after complete callosotomy and, possibly, modest enhancement of intrahemispheric FC.

Limits of the present study.

A limitation of this study is the hand classification of independent components as signal of interest or artefact, in that it could be affected by errors due to inexperience in the field. However, this procedure is preferred respect to the automatic classification because the data set here analysed correspond to a group of subjects with altered neural activity, and therefore, some components that corresponding to valid RNSs could be unrecognized and classified as a noise. Another limit of this study is the temporary impossibility to perform a comparison with a healthy control group and therefore the 2nd level analysis between groups to give statistical significance to the results could not be performed.

Conclusion.

In conclusion, it can be inferred that the CC is necessary for a correct interhemispheric functional connectivity, for example to have a bilateral neural activity in some networks as the DMN and the frontoparietal right and left. At the same time, the interhemispheric connectivity maintained in the networks related to the visual area suggests the presence of subcortical path that allows to transfer the information between the hemispheres.

Since split-brain patients are rare, since the complete callosotomy surgery as treatment for sever epilepsy has been replaced by drug interventions, and most of them have aged, it will be difficult to further study interhemispheric FC in this group of subjects. A future development could be the analysis and comparison with a healthy control group to give some statistical significance. Moreover, the FC could also be studied using other technique, such as the seed-based analysis. Another idea could be to study the structural connectivity associated to the FC using the Diffusor Tensor Imaging (DTI) technique, to investigate if any subcortical pathway is present in the split-brain patients.

Bibliography

Andersson JLR, Jenkinson M, Smith S. Non-linear registration, aka spatial normalisation. FMRIB technical report TR07JA2, 2010.

Barkhof F, Haller S, Rombouts S. Resting-State Functional MR Imaging: A New Window to the Brain. Radiology, 272 (1): 29-49, 2014.

Beckmann CF, DeLuca M, Devlin JT, Smith SM. Investigations into resting-state connectivity using independent component analysis. Philosophy Transaction of Royal Society B, 360: 1001-1013, 2005.

Beckmann CF. Modelling with independent components. NeuroImage, 62: 891-901, 2012.

Beckmann CF, Smith SM. Probabilistic Independent Component Analysis for Functional Magnetic Resonance Imaging. Transactions on Medical Imaging, 23 (2): 137-152, 2004.

Bijsterbosch J, Smith SM, Beckmann C. Introduction to Resting State fMRI Functional Connectivity. Oxford University Press, 2017.

Biswal B, Yetkin FZ, Haughton VM, Hyde JS. Functional connectivity in the motor cortex of resting human brain using echo-planar MRI. Magnetic Resonance in Medicine, 34 (4): 537-541, 1995.

Broca P. Sur le siège de la faculté du langage articulé. Bulletins et Mémoires de la Société d'Anthropologie de Paris, 6 (1): 377-393, 1865.

Formisano E, Di Salle F, Goebel R. Fundamentals of Data Analysis Methods in Functional MRI. Advanced Image Processing in Magnetic Resonance Imaging, 481-503, 2005.

Fox MD, Raichle ME. Spontaneous fluctuations in brain activity observed with functional magnetic resonance imaging. Nature Reviews Neuroscience, 8: 700-711, 2007.

Gazzaniga MS, Bogen JE, Sperry RW. Observations on visual perception after disconnexion of the cerebral hemispheres in man. Brain, 88 (2): 221-236, 1965.

Goebel R, Jansma H, Eck J. BrainVoyager QX Getting Started Guide (version 2.13 for BVQX 2.8). Brain Innovation B.V.

Gore JC. Principles and pratice of functional MRI of the human brain. The Journal of Clinical Investigation, 112: 4-9, 2003.

Greve DN, Fischl B. Accurate and robust brain image alignment using boundary-based registration. Neuroimage, 48 (1): 63-72, 2009.

Griffanti L, Douaud D, Bijsterbosch J, Evangelisti S, Alfaro-Almagro F, Glasser MF, Duff EP, Fitzgibbon S, Westphal R, Carone D, Beckmann CF, Smith SM. Hand classification of fMRI ICA noise components. NeuroImage, 154: 188-205, 2017.

Hung SC, Lee CC, Chen HH, Chen C, Wu HM, Lin CP, Peng SJ. Early recovery of interhemispheric functional connectivity after corpus callosotomy. Epilepsia, 60: 1126-1136, 2019.

Jenkinson M, Bannister P, Brady JM, Smith SM. Improved Optimisation for the Robust and Accurate Linear Registration and Motion Correction of Brain Images. NeuroImage, 17 (2): 825-841, 2002.

Jenkinson M, Pechaud M, Smith SM. BET2: MR-based estimation of brain, skull and scalp surfaces. In: Eleventh annual meeting of the organization for Human Brain Mapping, 17: 167, 2005.

Jezzard P, Matthews PM, Smith SM. Functional Magnetic Resonance Imaging: An Introduction to Methods. Oxford : Oxford University Press, 2001.

Johnston JM, Vaishnavi SN, Smyth MD, Zhang D, He BJ, Zempel JM, Shimony JS, Snyder AZ, Raichle ME. Loss of Resting Interhemispheric Functional Connectivity after Complete Section of the Corpus Callosum. The Journal of Neuroscience, 28 (25): 6453– 6458, 2008.

Laird AR, Robinson JL, McMillan KM, Tordesillas-Gutierrez D, Moran ST, Gonzales SM, Ray KL, Franklin C, Glahn DC, Fox PT, Lancaster JL. Comparison of the disparity between Talairach and MNI coordinates in functional neuroimaging data: Validation of the Lancaster transform. Neuroimage, 51: 677-683 (2010).

Lancaster JL, Tordesillas-Gutiérrez D, Martinez M, Salinas F, Evans A, Zilles K, Mazziotta JC, Fox PT. Bias between MNI and Talairach coordinates analyzed using the ICBM-152 brain template. Human Brain Mapping, 28 (11): 1194-1205, 2017.

Lienhard DA. Roger Sperry's Split Brain Experiments (1959-1968). Embryo Project Encyclopedia, 2017.

McCarthy P. FSLeyes (1.2.0). Zenodo, 2021.

Ogawa S, Lee TM, Kay AR, Tank DW. Brain magnetic resonance imaging with contrast dependent on blood oxygenation. Proceedings of the National Academy of Sciences, 87: 9868-9872, 1990a.

Osawa S, Lee TM, Nayak AS, Glynn P. Oxygenation-sensitive contrast in magnetic resonance image of rodent brain at high magnetic fields. Magnetic Resonance in Medicine, 14: 68-78, 1990b.

Owen JP, Li YO, Yang FG, Shetty C, Bukshpun P, Vora S, Wakahiro M, Hinkley LBN, Nagarajan SS, Sherr HE, Mukherjee P. Resting-State Networks and the Functional Connectome of the Human Brain in Agenesis of the Corpus Callosum. Brain Connectivity, 3 (6): 547-562, 2013.

Pauling L, Coryell CD. The Magnetic Properties and Structure of Hemoglobin, Oxyhemoglobin and Carbonmonoxyhemoglobin. Proceedings of the National Academy of Sciences (USA), 22 (4): 210-216, 1936.

Pearce JMS. The "split brain" and Roger Wolcott Sperry (1913-1994). Revue Neurology (Paris), 175 (4): 217-220, 2019.

Poldrack R, Mumford J, Nichols T. Handbook of Functional MRI Data Analysis. Cambridge University Press, 2011.

Robert E, Kelly Jr, Alexopoulos GS, Wang Z, Gunning FM, Murphy CF, Morimoto SS, Kanellopoulos D, Jia Z, Lim KO, Hoptman MJ. Visual inspection of independent components: Defining a procedure for artifact removal from fMRI data. Journal of Neuroscience Methods, 189: 233-245, 2010.

Roland JL. Snyder AZ., Hacker CD., Mitra A., Shimony JS., Limbrick DD., Raichle ME., Smyth MD., Leuthardt EC. On the role of the corpus callosum in interhemispheric functional connectivity in humans. Proceedings of the National Academy of Sciences, 114 (50): 13278-13283, 2017.

Sperry RW. Hemisphere deconnection and unity in conscious awareness. American Psychologist, 23 (10): 723-733, 1968.

Sperry RW. Cerebral Organization and Behavior: The split brain behaves in many respects like two separate brains, providing new research possibilities. Science, 133(3466): 1749-1757, 1961.

Siero JCW. Bhogal A., Jansma JM. Blood Oxygenation Level–dependent/Functional Magnetic Resonance Imaging. PET Clinics, 8 (3): 329-344, 2013.

Smith SM, Jenkinson M, Woolrich MW, Beckmann CF. Advances in functional and structural MR image analysis and implementation as FSL. NeuroImage, 23: S208-S219, 2004.

Smith SM, Fox PT, Millerm KL, Glahn DC, Fox PM., Mackay CE, Filippini N, Watkins KE, Toro R, Laird AL, Beckmann CF. Correspondence of the brain's functional architecture during activation and rest. Proceedings of the National Academy of Sciences (USA), 106 (31): 13040-13045, 2009.

Smith SM, Jenkinson M, Woolrich MW, Beckmann CF, Behrens TEJ, Johansen-Berg H, Bannister PR, De Luca M, Drobnjak I, Flitney DE, Niazy R, Saunders J, Vickers J, Zhang Y, De Stefano N, Brady JM, Matthews PM.

Advances in functional and structural MR image analysis and implementation as FSL. NeuroImage, 23(S1): 208-219, 2004.

Talairach J, Turnoux P. Co-Planar Stereotaxic Atlas of the Human Brain: 3-Dimensional proportional system: An approach to cerebral imaging. Thieme Medical Publishers, Inc. New York, USA, 1988.

Tianming L, Kaiming L, Lei Guo, Jingxin N, Gang L. Review of methods for functional brain connectivity detection using fMRI. Computerized Medical Imaging and Graphics, 33: 131-139, 2009.

Tyszka JM, Kennedy DP, Adolphs R, Paul LK. Intact Bilateral Resting-State Networks in the Absence of the Corpus Callosum. The Journal of Neuroscience, 31 (42): 15154-15162, 2011.

Uddin LQ, Mooshagian E, Zaidel E, Scheres A, Margulies DS, Clare Kelly AM, Shehzad Z, Adelstein JS, Castellanos FX, Biswal BB, Milham MP. Residual functional connectivity in the split-brain revealed with resting-state functional MRI. Behavioral, Integrative and Clinical Neuroscience, 19 (7):703-709, 2008.

Van Wagenen WP, Herren RY. Surgical division of commissural pathway in the corpus callosum: relation to spread of an epileptic attack. Archives of Neurology & Psychiatry, 44 (4):740-759, 1940.

Ringraziamenti

A conclusione di questo elaborato vorrei ringraziare chi ha contribuito alla realizzazione dello stesso.

Un ringraziamento particolare va alla mia relatrice Mara Fabri che mi ha seguito, con infinita disponibilità e pazienza, fino alla fine dell'elaborato.

Grazie anche al mio correlatore Gabriele Polonara per avermi dato la possibilità di svolgere il tirocinio, che ha portato alla stesura di questa tesi, presso il suo dipartimento.

Un ringraziamento va anche a Marco Valenti e Luca Reversi per il loro prezioso aiuto.

Ringrazio infinitamente la mia famiglia perché senza il vostro supporto questo lavoro di tesi non esisterebbe nemmeno.

Grazie a tutti i miei colleghi di corso, coinquiline, e a tutti gli amici con cui ho condiviso momenti di spensieratezza e gioia.

Ultimo ma non per importanza, ci tengo a ringraziare il mio fidanzato Antonio per avermi supportata/sopportata e accompagnata durante questo percorso. Grazie.